eBike Radars for Increased Safety

Andreas Thoft and Rebecka Lindquist

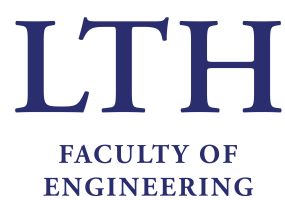

Master's Thesis
Biomedical Engineering
Faculty of Engineering LTH
Department of Biomedical Engineering
Supervisor: Frida Sandberg
In Collaboration with Robert Bosch AB
Lund, June 2020

Abstract

The purpose of this thesis is to develop a blind spot detection system for increased safety and comfort for a biker. The solution is based on power-efficient small A111 radars, developed by Acconeer AB, which have a range up to seven meters while consuming only a few milliwatts.

Sensor evaluation is performed for the intended use and from this, concepts are generated. These are tested to obtain the number of sensors, choice of dielectric lens, the angling and the placement needed for the final prototype. User cases representing the intended use of everyday biking are defined and recorded with the final prototype. Lastly, algorithms are tested to increase the accuracy and robustness of the blind spot detector.

The final prototype consists of three A111 sensors placed under the saddle and are angled 30° horizontally apart and with the range up to seven meters. The three user cases were recorded with increasing difficulty, resulting in one training and one test set which was validated through video recording to obtain ground truth. The blind spot detector performance for the range up to seven meters resulted in the accuracy of 89%. The specificity was close to 95% but the sensitivity was low on the most difficult user case which show limitations mostly in the far range. This result was obtained using the associated sparse sensor processing with added CFAR and correlation of frames for increased robustness.

The results show that the A111 radar sensor can be used for a blind spot detection system but with a somewhat shorter range than tested. More testing is required to improve the detectability and range further through the optimization of both the prototype and the proposed algorithms.

Acknowledgments

Firstly, we want to thank our supervisor at the Department of Biomedical Engineering at LTH, Frida Sandberg, for all help and guidance during the thesis.

We would also like to thank the people helping us during the project at Robert Bosch AB where we spent most of our time during this thesis. A special thanks to our supervisor Gustav Träff for the help and guidance during our work. We have appreciated the freedom within the thesis which made it possible to adapt and complete the work.

Furthermore, we also want to show appreciation to Acconeer AB, for guiding us in the right direction in the beginning of the project and answering questions.

We have really enjoyed the project and we are happy to have been able to meet so many inspiring people. The thesis made us gain knowledge in new areas and it has been interesting to complete the full development process, from sensor evaluation and finding suitable applications resulting in a final functioning prototype.

Andreas Thoft & Rebecka Lindquist

List of Acronyms and Abbreviations

CA-CFAR Cell-Average Constant False Alarm Rate

CFAR Constant False Alarm Rate

CUT Cell Under Test

E-Plane Elevation-Plane

eBike Electronic Bike

H-Plane Horizontal-Plane

HPBW Half Power Beam Width

Lidar Light Detection and Ranging

MCU Micro-Controller Unit

PCR Pulsed Coherent Radar

PRF Pulse Repetition Frequency

Radar Radio Detection And Ranging

RCS Radar Cross Section

RSS Radar System Software

SNR Signal to Noise Ratio

Contents

Chapter 1
Introduction

Different types of safety systems are possible depending on the position and type of sensors. Common systems in cars for increased safety are parking aid, adaptive cruise control, blind spot surveillance and rear-end collision warnings. These systems aim to prevent accidents by informing or helping the driver to avoid dangerous situations. The systems are more or less complex, e.g. mare blind spot detection does not meet the same high-performance requirements as cruise control, which needs both faster update rate and resolution.[1]

Modalities such as radar, ultrasound, lidar and cameras are all used in the different safety systems. However, all mentioned modalities have certain characteristics which may introduce some limitations of the sensors. For example, the range of ultrasonic sensors is limited and camera systems are quite sensitive to the conditions of the environment [2, 3]. Radar sensors can have a large range, are insensitive of being covered by dirt and different weather conditions. However, the most common types of radars usually has a quite large energy consumption.

Companies, such as Nireeka and Calamus which manufacture eBikes, use built-in ultrasonic sensors for detecting approaching targets and for blind spot surveillance. The biker is then notified through either haptic feedback in the handlebars or by visual feedback on a display when a target is present.[4, 5]

Klotz [6] describes that radar sensors, which are well known to be used in the car industry, can be used for parking aid, adaptive cruise control, blind spot surveillance and pre-crash systems. Garmin Varia is a product which functions as blind spot surveillance for bikes using only one radar. The product is attachable to the bike and gives notifications to the biker of approaching targets. Since it is only one sensor, the system gives no indication other than the range to the target and cannot tell if the target approaches to the right or to the left [7].

Safety systems for bikes needs smaller, more energy-efficient and cheaper

Figure 1.1: To the left the definition of the visual span can be seen. To the right, the definition of the blind spot of a biker according to the definition of the visual span can be seen.

sensors compared to those in cars and other vehicles. This is due to the prerequisites of bikes and eBikes which have both limited space and available power.

When the biker needs to make a drastic turn or want to control if there is someone behind, the only way to do so is to turn the head and torso backwards. When changing the direction of the upper body an unintentional change of direction and wobble may occur. The biker also removes the attention from the road ahead. The blind spot of a biker is limited to the human vision. The human vision covers an area of approximately 200° to 220° degrees, defined as in the left illustration in figure 1.1. Hence the visual blind spot range from 140° to 160° [8], see the right illustration in figure 1.1 as seen from above for a 160° blind spot. The bike does not have mirrors or any other solutions to make it possible to visually cover both sides and backwards. One of the more simple systems for increased safety which can handle this problem is blind spot surveillance.

The purpose of this thesis is to evaluate if the A111 radar sensor from the company Acconeer AB can be used to increase the safety of an eBike in a blind spot detection system. The aim is to develop a concept which, if proven possible, can be tested and evaluated. The limitation of the used sensor need to be examined to determine if the maximal range and the shape of the radar beam would suit the application. Furthermore, the specifications of the desired system, i.e. the number of sensors needed and placement of the sensors, needs to be determined. Hence, different concepts should be generated and evaluated. Lastly, to evaluate if a robust detection system could be possible, a presence detection algorithm is evaluated and improved to increase the robustness.

The report includes background information regarding common radar systems (Sec 2.1), the used radar sensor (Sec 2.2 and 2.3) and the different algo-

rithms suggested to make the blind spot detector more robust (Sec 2.4). Then the method of the evaluation of the sensor (Sec 3.1), concept generation and evaluation (Sec 3.2), data acquisition (Sec 3.3) and lastly the detector optimization is described (Sec 3.4). Lastly, the results are presented (Sec 4.1-4.4) and then discussed (Sec 5.1-5.5).

Chapter 2
Background

This chapter gives a general introduction to radar technology and its application to blind spot detection (Sec 2.1). This is followed by a description of the radar sensor used in the present project (Sec 2.2) and its properties to produce different types of frames of the recorded scenes (Sec 2.3). Furthermore, the algorithms used for robust blind spot detection are described in section 2.4.

2.1 Radar

Radars are used in many different areas. There are two different main types of radars, continuous-wave radar and pulsed radar. The main principle of almost all radars is that the distance to objects is determined by calculating the time of flight of the transmitted pulse. The transmitted pulse travels with the speed of light and, if the time of flight can be measured, the distance to the reflecting object can be determined. The behaviour and propagation of the radar pulses transmitted can be described by the radar equation. Different radars are usually described by the possible range and the angular spread of the radar beam. These properties affects the possible usage of the specific radar sensor.

2.1.1 Radar equation

The detection of a target using radar technique requires that the signal to noise ratio, SNR, must be high enough for the target to be distinguishable with some certainty. The radar equation describes the relationship between the transmitted and received power.

The radar pulse path from the transmitter and back to the receiver can be modelled by the two-way radar equation for a monostatic setup, i.e. the

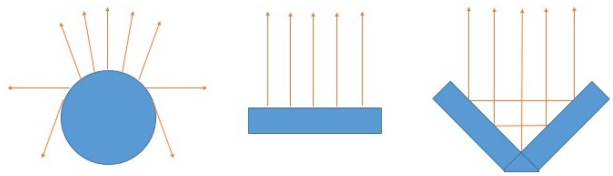

Figure 2.1: The directivity of a sphere, flat plate and a corner reflector. A sphere has low directivity while a flat plate and corner reflector has higher. Based on the description of radar cross section by the Avionics Department [9].

transmitter and receiver are co-located. The equation for the peak power at the radar receiver, P_r, is given by equation 2.1, where P_t is the transmitted power, G_t and G_r is the transmitter and receiver antenna gain, λ is the wavelength, σ is the radar cross section, RCS, and R is the distance to the target. This equation assumes that the target is within the field of view of the radar. [9]

$$P_r = \frac{P_t G_t G_r \lambda^2 \sigma}{(4\pi)^3 R^4} \tag{2.1}$$

While the G_t, G_r and λ are radar specific parameters, σ and R depend on the target. The RCS represents the ability for the radar beam to be reflected back to the receiver. It is dependent on the effective area of which the target within the radar illumination, the reflectivity and the directivity of the target. The directivity is different for different shapes due to its geometry and therefore the property to not scatter the radar pulses away but rather towards the receiver again. A sphere scatter the beam much more than a plate which can redirect the radar pulses back towards the receiver again. This can be seen in figure 2.1 where some geometrical figures are displayed with its directivity. [9]

The reflectivity depends heavily on the characteristics of the surface and in which media the radar pulses travel. This factor is a value between zero and one, where one means that the surface is a perfect reflector. The reflectivity factor is often bundled together with the RCS. In equation 2.2 the reflectivity, γ, of the two boundary materials is described as a function of the two refractive indexes, n, which is dependent on the wavelength of the transmitted radar. This can also be expressed by the permittivity of the materials in which medium the light porpagates in, ϵ and the permittivity in free space, ϵ_0. For a nonmagnetic material the refractive index is $n = \sqrt{\frac{\epsilon}{\epsilon_0}}$, and equation can be simplified into the right part of equation 2.2.

$$\gamma = (\frac{n_1 - n_2}{n_1 + n_2})^2 = (\frac{\sqrt{\epsilon_1} - \sqrt{\epsilon_2}}{\sqrt{\epsilon_1} + \sqrt{\epsilon_2}})^2 \tag{2.2}$$

Furthermore, the direction of the objects own vertical axis is of importance. Meaning, a tilted plate would at certain angles scatter the radar pulses away from the receiver. Hence, the RCS is also dependent on the angle of the object and consideration of this angle must be taken into account. [9]

The material used to cover the transmitter and receiver is required to have a low reflectivity for it to not interfere with the radar pulses which would result in loss of signal power or false detection. Acconeer lists in its radar documentation [10] approximate values of the relative permittivity and reflectivity for common materials. According to the documentation, metals have a reflectivity of $\gamma = 1$ meaning that it reflects all radar waves of this wavelength while human skin only has $\gamma = 0.22$.

In the radar equation 2.1 it is common to rewrite the radar specific constants such as G_t, G_r, λ, unexplained losses and other constants into one, C, called the radar loop gain. By reformulating the radar equation in the logarithmic form a more simple equation is obtained. In the report *Radar Loop Gain Measurements* the authors [11] express the SNR in dB according to equation 2.3.

$$SNR = C + \sigma - 4R \tag{2.3}$$

The constant C is the radar loop gain, σ is the RCS which is comprised to contain the reflectivity, directivity and effective area of the target and R is the range to the target. The radar loop gain, C, needs to be known, however, it is hard to estimate and the value is usually determined by empirical measurements [11]. However, the most important influence on the detectability is the distance to the target where for a small distance increase leads to a large loss of SNR.

2.1.2 Continuous wave radar

Continuous wave radar has one transmitter and one receiver to continuously send and receive pulses. It is commonly used as a short-range radar. The distance to the object cannot be determined using continuous wave radar since the information from different ranges cannot be distinguished in time. To attain more information about depth, frequency modulation is a common approach. By modulating the frequency of the transmitted pulse in time, the range can also be determined due to the time-resolution added. The Doppler

shift, or frequency shift, due to movements of the targets, gives information about the velocity and heading direction of the object.[12]

2.1.3 Pulsed radar

Pulsed radar is another type of radar, where the same antenna functions as both transmitter and receiver. It is better suited for long-range detection due to the isolation between the transmitted signal and received signal. No modulation is needed as the time of flight can be determined directly. The velocity of targets can be determined using the Doppler effect. However, one disadvantage is that there will be a blind spot for certain speeds due to aliasing. This effect is known as Doppler ambiguities and is affected by the pulse repetition frequency, PRF. The targets sampled at PRF causes aliasing at multiples of the PRF, hence Doppler frequencies which correspond to integer multiples of PRF will be indistinguishable.[12]

2.1.4 Pulsed Coherent Radar

Pulsed coherent radar, PCR, is a less common type of radar. The technology is both patented and developed by the company Acconeer AB. The idea is to gain the advantages from both the continuous wave and the pulsed radar, i.e. both low energy consumption similar to pulsed radar but with the high accuracy as continuous wave radar. This is made possible due to one transmitting and one receiving antenna, just as the continuous wave radar, but sending the pulses the same way as the pulsed radar. The distance to the target can be determined by the time of flight without any modulation. The coherency of the radar comes from the fact that each pulse has a reference of the time and phase. This results in high accuracy similar to the one when using continuous wave radar.[10, 13]

2.2 Sensor specifications

Acconeer has developed a small PCR-sensor with a low power consumption of a few milliwatts and low cost. The so-called A111 radar sensor, with the XM112 module together XB112 breakout board used for quick setup and evaluation of the sensor, was chosen for this thesis for these properties. A picture of the sensor can be seen in figure 2.2.

The sensor transmitts pulses which have a carrier frequency of 60 GHz [10]. These pulses, also known as wavelets, can either be long or short depending on the duration of the waves transmitted with the carrier frequency

Figure 2.2: The A111 sensor mounted on the XM112 module. The module is in turn mounted on the XB112 breakout board. To the left are two micro-USB connectors.

unchanged. The length of the wavelet is configured by choosing a so-called profile, i.e. profile 1 to 5. The longer the wavelet, e.g. profile 5, the more energy is transmitted resulting in a higher SNR but decreased depth resolution. The depth resolution is approximated in equation 2.4 where t_{pulse} is the duration of the wavelet in time and v the speed of light in the propagation medium. The measured signal of the sensor holds information about the reflection from targets but also noise from e.g. background clutter and scattered pulses.

$$d_{res} \approx \frac{t_{pulse} v}{2} \tag{2.4}$$

If more energy of each wavelet is transmitted then the range for detecting a target can be increased due to higher SNR. Acconeer state average ranges for the sensor for which typical targets are detectable. For example, a human torso is detectable up to the distance of 2 meters without lens and 5 meters with lens, when profile 2 and envelope service is used [10]. The software of the evaluation kit limits the maximal range to a maximum of 7 meters.

With the module comes open-source code to run an exploration tool to visualize and process the radar data [10]. The exploration tool also contains a graphical user interface, GUI. The GUI enables quick setup time for eval-

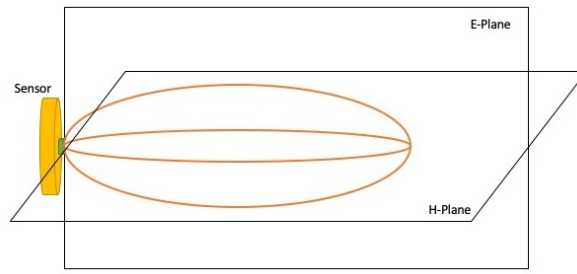

Figure 2.3: Visualization of the E-plane and the H-plane for the sensor transmitting pattern.

uation of sensor settings and replay of the data. Different services for data acquisition, which will be further explained in section 2.3, can be chosen before each recording and the data can be saved as H5-files. During the replayed in the GUI for post-processing tuning which also may be applied during the recording of data.

The radiation pattern of the A111 sensor's transmitter is defined by the elevation plane, E-plane, and the horizontal plane, H-plane. The visualization and definition of this can be seen in figure 2.3. The magnitude, expressed in dB, is described by a function of the angle in degrees. The highest directional power of the transmitted pulse is directly in front of the sensor and the magnitude then decline as the angle increases. In the sensor data-sheet, [14], the statistical results of the magnitude measurement indicates a half power beamwidth, HPBW, of $40°$ and $80°$ for the E-plane and H-plane respectively. This results in an almost coniform shape of the radar beam in front of the sensor.

In addition to the products which includes the radar sensor, different attachments are offered. Lenses of different types can be used to direct and amplify the radar beam. The lenses are mounted close to the sensor and can improve the range by several meters.[10] By using lenses the radiation pattern of the sensor can be altered. A lens holder can be mounted on the XB/XM112 evaluation kit which has different positions for the lenses. Provided in the lens kit are two types of lenses, a hyperbolic and a Fresnel lens, with similar characteristics. See figure 2.4 of the lenses and the lens holder. Using the hyperbolic lens in the D1 position, i.e. position closest to the sensor, the magnitude has a max gain of 5.8 dB in comparison to the free space scenario [15]. The E- and H-plane is decreased to $22°$ and $30°$ respectively since the HPBW is altered. The hyperbolic lens is the one which amplifies the radar pulses mostly and consequently increases the range the most.[10]

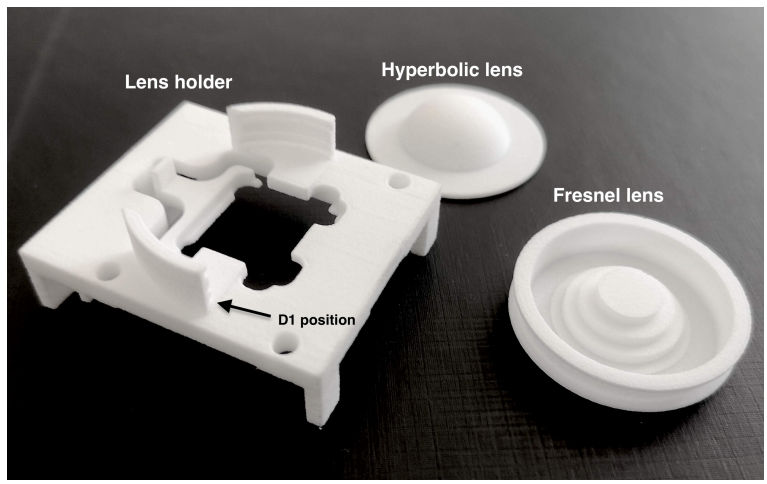

Figure 2.4: The lens holder together with the Fresnel lens and hyperbolic lens. The position called D1 is marked.

How fast a radar frame is sampled is a tunable sensor parameter leading to data frames per seconds, f_f, [Hz]. How fast the hardware can sample one frame depends on the used service and also on other parameters such as the range interval, downsampling factor, hardware accelerated average samples etc which will be further explained in the following paragraphs. Setting a too fast update rate could lead to that the sensor doesn't have time to construct a frame in time until it needs to sample the next. This results in missed frames since the sensor skips frames until it is finished and ready to sample the next. The sampling method of the sensor can be set to be either sensor or host driven. This determines how and when the frame is sampled, either when the microcontroller unit, MCU, or when the sensor board itself demands it.

The hardware accelerated average samples parameter, HWAAS, is the amount of samples that are averaged to obtain a single point in the data. This is done directly on the hardware and not in the MCU. This will therefore not influence the processing time, it rather increase the time it takes to measure a frame. However, an increase of the HWAAS leads to higher radar loop gain resulting in a higher detectability over the background noise.[10]

Sensor leakage occurs as the sensor tries to measure the returning radar pulses from depths too close to the sensor. This happens since the transmitter and receiver are closely aligned resulting in that the receiver detects the pulses transmitted directly from the transmitter. As an increase in profile leads to a larger pulse time, t_{pulse}, the direct leakage occurs further out from the sensor. The direct leakage is a static disturbance and may be required to be filtered

out if one wants to measure this close to the sensor. One can overcome this effect by changing the range interval to start at the first depth without sensor leakage. [10]

2.3 Sensor data acquisition

The data acquisition from the A111 sensor is acquired from the Radar System Software, RSS, which produces the output data. The output data can either be raw or processed. The raw sensor data can be provided in four services; envelope, sparse, in-phase and quadrature (IQ), and power bins. The RSS also provides some processing evaluation code which is based on the data produced from the service. Envelope and Sparse service will be further described below. IQ service is similar to the Envelope service and provides information on both phase and magnitude of the returned radar pulses. It is used to detect very small movements. The power bin service is simply a depth binning version of the Envelope service, resulting in fewer depth points and lower resolution in the post-processing.

2.3.1 Envelope

The envelope service presents the sampled data of the received energy as a function of the distance and the real-valued amplitude is described by equation 2.5.

$$x(d) = A_d \tag{2.5}$$

A_d is the sampled energy received from a certain distance, d. The distance is defined by the time of flight. One frame generated by the envelope service consists of a depth sweep, $x(d)$, and is several radar pulses from which the energy content is measured from a set of time delays. The number of sampling points in the depth which one frame comprises depends on the recording depth and the depth resolution. The smallest depth interval is approximately 0.5 millimeters. By downsampling, this interval can be increased by a factor of two or four, i.e. approximately 1 and 2 millimeters [16]. The frame visualization can be seen in figure 2.5 along with the frame intensity output of the previous frames in time.

The measured energy returned from reflectors is also influenced by noise and to increase the SNR, the envelope service comes with an exponential smoothing filter. The frames are filtered in time for a certain depth [16]. The exponential averaging filter equation is adapted from Lasek et. al. [17]. The

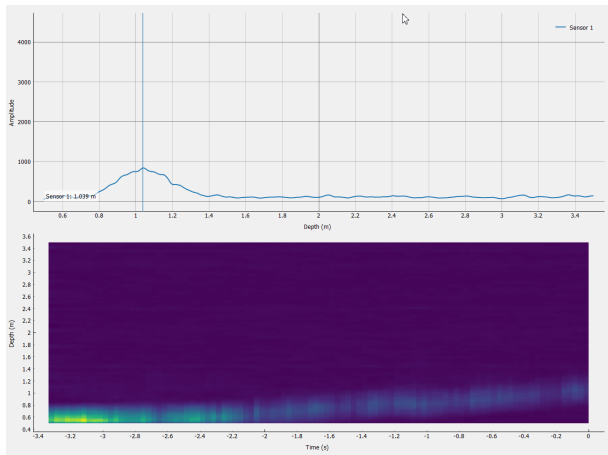

Figure 2.5: In the top figure is a envelope frame as amplitude as a function of depth. In the figure below is the frame output color coded in intensity for a frame along the y-axis and frames over time along x-axis.

initialization of the filter at $t = 0$ is set to $s_0(d) = x_0(d)$ and the filter is then updated according to equation 2.6.

$$s_t(d) = (1 - \alpha)x_t(d) + \alpha s_{t-1} \quad t > 0 \tag{2.6}$$

As can be seen from equation the running average factor, α, decides the level of filtering. A large α results in that a large weight on past inputs and a small one results in larger weight on the current radar frame input. When using a large α, objects moving fast from frame to frame will remain longer.

The envelope service has its frames sampled several times along the depth which results in large amount of data for each frame. The amount of data and the time to construct a frame is influenced by the range interval and the downsampling factor. For a too large range the rate of which the sensor can produce the frames is influenced and if set to large it may result in missed frames.

2.3.2 Sparse

A sparse frame is different from the frames of the other services since it consists of several sweeps per frame. Furthermore, the sparse service is sampled very seldom, approximately every 6^{th} centimeter, rather than several times per wavelength. The data from the sparse service can be described by $x(f, s, d)$ where

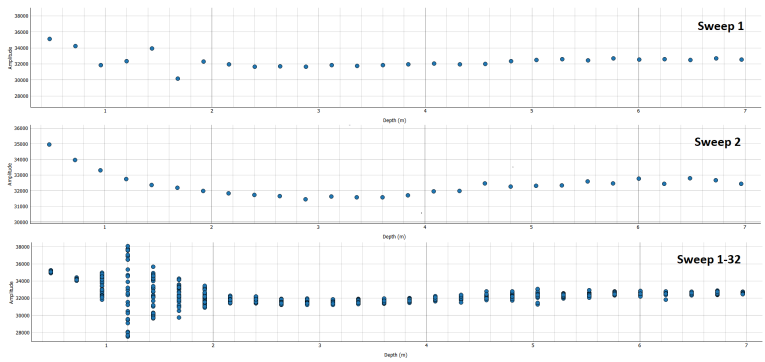

Figure 2.6: Visualization of raw sparse data output. Top figure is the first sweep in a certain frame. In the middle is the consecutive sweep and at the bottom is the entire sparse frame containing all 32 sweeps.

f denotes the sampled frame, s the sweep index and d the range depth point. The sparse service is designed for situations where one wants to record dynamic targets. The service is very robust and has a low power consumption which comes from the sparsely placed sampling points. This service also has the capability of downsampling which reduces the number of depth point along the set range. A downsampling factor of two results in that the depth points are spaced every 12^{th} centimeter instead and therefore reduces the amount of data.

A moving object which is captured within one frame will result in that the sweep amplitude at a certain depth point will alter. Looking at one certain depth this leads to large intra-frame differences, i.e. high variance in the sweep amplitudes as a result of the movement. For static objects, the sweeps will instead be constant for each frame and therefore the intra-frame variance is low.

A visualization of the raw data output from the sparse service can be seen in figure 2.6. The figure on top is the first sampled sweep, i.e. $x(f = 1, s = 1, d)$, and the second figure is the consecutively sampled sweep, $x(f = 1, s = 2, d)$. All of the sweeps, i.e. 32 sweeps, are then combined into one frame, $x(f = 1, s, d)$, which is visualized in the final figure at the bottom. One can see that moving targets within a frame at a certain depth, d, has a large variance in its sweep values. This can be seen at depth d = 1.25 m, where the values is largely spread compared to depth d = 3.5 m which is more compact.

With the Sparse service, it is possible to set a higher frame rate, f_f, as it generally produces less data. The f_f typically ranges from 1 to 200 Hz and depends on the number of sweeps per frame, depth, downsampling factor etc. The frame sampling rate is represented by the parameter called sweep rate f_s.

The sweep rate can be set between 1 to 50 kHz. Depending on these two configurations the sensor can perform a nearly 100% duty cycle, but with the cost of high power consumption. What makes the Sparse service desirable is the lower duty cycle performing with lower power consumption and produce less amount of data.

The Sparse service also comes with the configuration of setting the sampling mode and changes the way the hardware accelerated averaging is done. The two modes A and B affect the SNR, where B is optimized for maximal SNR and is suitable for applications where one wants to see movements over long ranges. Sampling mode A is instead better for gesture recognition, measuring the distance to a movement and speed measurements close to the sensor. [18]

2.4 Algorithms for robust detection

2.4.1 Sparse presence detection

A static target generates a strong reflection in the sparse data at the same depth for every sweep within the frame. For a dynamic target, the change of depth within the frame instead results in e.g. high amplitude in the first sweep and the consecutive has low. From this description of the raw data, Acconeer propose two algorithms in the exploration tool for detecting both slow and fast movements [19]. Since the sweep rate is very fast, a large spread in the sweep data within a frame indicates that a fast movement at this depth has occurred. Slower movements are instead detected between two frames since the frame rate is much slower than the sweep rate. In other words, the slower movements are captured by the inter-frame deviation and the faster by the intra-frame deviation. The noise power is estimated to make the algorithm more resistant to noise and also to normalize the detection levels.

Intra-frame deviation

As previously mentioned, the intra-frame deviation, s_{intra}, is based on the sample standard deviation of the sweeps at a specific depth point within one frame. From the raw data, $x(f, s, d)$, the metric for this deviation is calculated using equation 2.7. The absolute difference between each sweep and the mean sweep is summarized and then normalized with a factor containing the number of sweeps, N_s. The mean sweep, $\mu(f, d)$, is calculated using equation 2.8.

$$s_{intra}(f,d) = \frac{1}{\sqrt{N_s(N_s-1)}} \sum_{s=0}^{N_s} |x(f,s,d) - \mu(f,d)| \tag{2.7}$$

$$\mu(f,d) = \frac{1}{N_s} \sum_{s=0}^{N_s} x(f,s,d) \tag{2.8}$$

For s_{intra} to become more stable it is low pass filtered by an exponential filter described by equation 2.9. This filtered version yields the output of $\bar{s}_{intra}$. The parameter α_{intra} is a tunable smoothing factor which is dependent on a time constant parameter. The time constant, τ_{intra}, is used to determine the α according to equation 2.10, where f_f is the frame sampling frequency. Hence, α_{intra} is a measure of how much weight to put on the latest output value, where a larger time constant leads to a more smoothed signal. If the output is too slow and sluggish the α_{intra} needs to be smaller to put more weight on the current s_{intra}. [19]

$$\bar{s}_{intra}(f,d) = (1-\alpha_{intra})s_{intra}(f,d) + \alpha_{intra}\bar{s}_{intra}(f-1,d) \tag{2.9}$$

$$\alpha = exp(-\frac{1}{\tau f_f}) \tag{2.10}$$

Inter-frame deviation

The inter-frame deviation algorithm is based on the assumption that slow movements do not have time to generate a change in the amplitude within one frame. The mean of all sweeps is calculated according to equation 2.8. The mean is then copied and filtered using an exponential averaging filter with α being tuned with different cutoff frequencies, one resulting in α_{fast} and the other in α_{slow}. In equation 2.11 and 2.12 one can see the resulting calculation of the two mean, which yields one fast, $\bar{\mu}_{fast}(f,d)$, and one slow, $\bar{\mu}_{slow}(f,d)$, part.

$$\bar{\mu}_{slow}(f,d) = (1-\alpha_{slow})\mu(f,d) + \alpha_{slow}\bar{\mu}_{slow}(f-1,d) \tag{2.11}$$

$$\bar{\mu}_{fast}(f,d) = (1-\alpha_{fast})\mu(f,d) + \alpha_{fast}\bar{\mu}_{fast}(f-1,d) \tag{2.12}$$

The cutoff frequency of the exponential averaging filter is transformed into α so that a 3 dB magnitude decrease of the filter is obtained at the cutoff

frequency. This is further described by Acconeer in their documents and the transformation is made using equation 2.13, where f_c is the desired cutoff frequency and f_s the sampling frequency. This is used for when $f_c < f_f$ and otherwise α is set to zero. Choosing one large and one small cutoff frequency thereby yields α_{fast} and α_{slow}.

$$\alpha = 2 - cos(2\pi f_c/f_s) - \sqrt{cos^2(2\pi f_c/f_s) - 4cos(2\pi f_c/f_s) + 3} \quad (2.13)$$

Once both the $\bar{\mu}_{fast}(f,d)$ and $\bar{\mu}_{slow}(f,d)$ have been obtained, the inter frame deviation, S_{inter}, is determined by taking the absolute difference according to equation 2.14. The absolute difference is then normalized with the constant $\sqrt{N_s}$, where N_s is the number of sweeps per frame. Similar to S_{intra}, the S_{inter} measure is filtered using a exponential averaging filter with a smoothing factor, α_{inter}, which also is tunable by the time constant τ_{inter} according to equation 2.10. This finally yields the inter-frame part, $\bar{s}_{inter}(f,d)$. [19]

$$s_{inter}(f,d) = \sqrt{N_s}|\bar{\mu}_{fast}(f,d) - \bar{\mu}_{slow}(f,d)| \quad (2.14)$$

Noise level estimation

Noise level estimation is used to normalize the detection levels so that the processing output becomes more invariant to high-frequency noise. It is assumed that the high-frequency components consist of random noise and objects moving unreasonably fast for the application. Therefore, this can be normalized since targets of interest generally will not generate any high-frequency components. To normalize against the high-frequency components depthwise, each depth channel needs to produce a measure of the quantity of the high-frequency components. The noise level estimation is performed by using a first-order differential filter three times, $N_{diff} = 3$, on the sweeps within a frame at a certain depth $x(f,s,d)$. The three differential equations are described in 2.15 with the output $x'''(f,s,d)$ from which the mean absolute deviation, $\hat{n}(f,d)$, is calculated according to equation 2.16.

$$\begin{aligned} x'(f,s,d) &= x(f,s,d) - x(f,s-1,d) \\ x''(f,s,d) &= x'(f,s,d) - x'(f,s-1,d) \\ x'''(f,s,d) &= x''(f,s,d) - x''(f,s-1,d) \end{aligned} \quad (2.15)$$

$$\hat{n}(f,d) = \frac{1}{N_s - N_{diff}} \sum_{s=1+N_{diff}}^{N_s} |x'''(f,s,d)| \quad (2.16)$$

The mean absolute deviation is then normalized according to equation 2.17 resulting in $n(f,d)$. This compensates the expected value for the differentiation. For a more stable metric, the exponential smoothing filter as previously described can be applied on $n(f,d)$ with the smoothing factor α_{noise}. This smoothing factor is a fixed parameter with a time constant of 1 seconds, which is calculated from equation 2.10. [19]

$$n(f,d) = \hat{n}(f,d) * \frac{1}{\sqrt{\sum_{k=0}^{N_{diff}} (\frac{N_{diff}!}{k!(N_{diff}-k)!})^2}} \tag{2.17}$$

Presence detection output

The algorithm combines the inter- and intra-frame part and normalizes it with the estimated noise level estimation to generate an output of the distance to the target. The output from the combination becomes the new signal, $\bar{s}_n(f,d)$, which is generated for each frame and is depth-dependent. The calculation to generate the output is given by equation 2.18, where the intra-frame weight, w_{intra}, decides the amount of contribution of the intra-frame part and $w_{inter} = 1 - w_{intra}$ weights the inter-frame part. w_{intra} spans between one and zero, where zero will set all weight on the inter-frame part and one will set all weight on the intra-frame part.

$$\bar{s}_n(f,d) = \frac{w_{inter}\bar{s}_{inter}(f,d) + w_{intra}\bar{s}_{intra}(f,d)}{\bar{n}(f,d)} \tag{2.18}$$

Once the output of the new signal, $\bar{s}_n(f,d)$, is generated, a depth filter is implemented by a running average operation over the full range within one frame. Due to the assumption that a target typically spans over several depth points, it will generate a more stable metric by having a running average. This operation is described in equation 2.19, where the signal is zero-padded outside the edges, i.e. for $d < 1$ and $d > N_d$. The number of depth points used in the average operation is set through the parameter $N_{average}$. If no running average needs to be performed this parameter can be put to one and then the output of $z(f,d)$ becomes equal to that of $\bar{s}_n(f,d)$.

$$z(f,d) = \frac{1}{N_{average}} \sum_{i=-N_{average}}^{N_{average}} \bar{s}_n(f,d+i) \tag{2.19}$$

To quantify the detection and at which depth the target is, the maximum value of $z(f,d)$ for this given depth, d, within a frame is stored. For the detection to be a bit more stable from frame to frame the value is put through

Table 2.1: Tunable parameters for the Sparse Presence Detection algorithm along with its units and limits.

Parameter	Description	Unit	Limits
τ_{intra}	Time constant for α_{intra}	s	[0, 0.5]
$f_{c(slow)}$	Cutoff frequency for α_{slow}, Inter-frame	Hz	[0.01, 1]
$f_{c(fast)}$	Cutoff frequency for α_{fast}, Inter-frame	Hz	[1, 100]
τ_{inter}	Time constant for α_{inter}	s	[0.01, 30]
w_{intra}	Amount of weight on intra-frame part	1	[0,1]
$N_{average}$	Number of depth points in running average	1	integer
τ_{output}	Time constant for α_{output}	s	[0.01, 30]
$v_{threshold}$	Detection threshold value	1	[0,5]

an exponential average filter. This is under the assumption that the object is not going in and out of frame. The amount of averaging is, as before, tuned with the parameter α_{output} which is set by the time constant τ_{output} according to equation 2.10. This smoothed value is then compared to a set constant threshold value and if the value exceeds this threshold a detection has occurred. The output from the presence detection algorithm provided by Acconeer is if a detection has occurred, the amplitude of the detection and at which depth the threshold has exceeded.

To summarize, the parameters for the sparse presence detection algorithm is presented in table 2.1 along with a small description, which unit and limits. This yields eight tunable parameters to optimize until the best detectability is acquired. [19]

2.4.2 Constant False Alarm Rate

The constant false alarm rate algorithm, CFAR, comes in a wide variety of configurations with the purpose to attain an adaptive threshold to detect targets in background clutter. An adaptive threshold, which is based on what the radar detects at the current frame, can achieve a lower rate of false detections when the background noise level is not constant. This is applicable for the cases of inter- and intra-frame noise variations.

The most simple version of CFAR is the so-called Cell-Averaging CFAR, CA-CFAR, where a cell represents one depth point. The purpose of the algorithm is to construct an average of the cells that surround the cell under test, CUT. This average is the noise level estimate of the surroundings of the target. All cells within a frame will be viewed as a CUT-cell which will result in

a threshold that is dependent on both the signal and index. The non-constant threshold will increase just before and after the target becomes the CUT-cell and then decrease at the target's center. This results in high contrast between the signal and the new adaptive threshold surrounding a target. To increase the contrast and to exclude the target in the noise estimate, so-called guard cells are used. Guard cells are not used in the averaging operation and the number of guard cells needed is depending on the width of the target. [20, 21]

CA-CFAR can be used on the data output from the sparse presence detection, $Z(f, d)$, to attain the new threshold, T_{CFAR}. CA-CFAR is applied on each frame, f, and the CUT-cell is dependent on depth, d. The threshold T_{CFAR} for a certain depth is calculated according to equation 2.20.

$$T_{CFAR}(f,d) = \frac{1}{2N_{CFAR} - N_{Edge}} \sum_{l=N_G+1}^{N_G+N_{CFAR}} (|Z(f,d-l)| + |Z(f,d+l|) \tag{2.20}$$

N_G is the number of guard cells that are included in the running average and N_{CFAR} is the number of cells used in the average on both sides of the CUT-cell. The signal $Z(f, d)$ is zero-padded and when the CUT-cell is located close to the edges the N_{Edge} parameter holds the number of cells that are inside the zero-padded part of the signal $Z(f, d)$. Hence, the cells on the edges will only have a noise estimate of one side. A summary of the algorithm is presented in figure 2.7, where one can see how the guard cells and the number of averaging cells are used to produce the threshold for the given CUT-cell. In the figure, the 10^{th} cell is under test to produce its threshold and is moving along the signal until $d = N_D$. This yields a threshold, T_{CFAR}, for each depth within a frame.

To not trigger on noise in a frame when no target is present or if the SNR is to low, a new constant threshold μ_{CFAR} is proposed. The difference, $\Delta(f, d)$, of $Z(f, d)$ and $T_{CFAR}(d, f)$ is calculated and if this $\Delta(f, d)$ exceeds this new constant threshold a detection has occurred. The visualization of the CFAR algorithm performance can be seen in figure 2.8. This yields the contrast between target and background noise which here is a simple DC component. The $\Delta(f, d)$ is large and positive for a detection and is small or negative for background clutter. The output of this implemented CA-CFAR detector is the maximal value of $\Delta(f, d)$ expressing at which depth the detection has occurred.

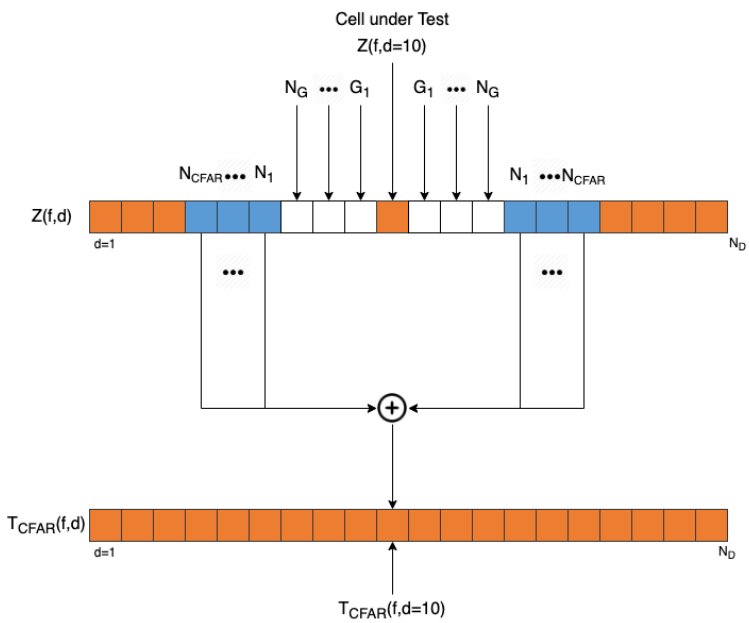

Figure 2.7: CFAR averaging operation with number of guard cells in white cells and the cell under average in the blue. This produces the threshold value for the orange CUT-cell.

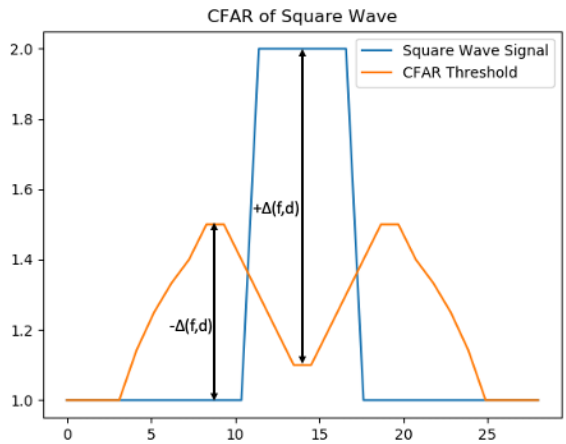

Figure 2.8: CFAR example of a square wave (target) in blue with a DC level. The orange is the CFAR threshold which is dependent on the depth. The subtraction of the depth points yield Δ which is largly postivie for a detection. The CFAR threshold was calculated using N_G = 2 and N_{CFAR} = 5.

2.4.3 Compensation of range

According to the radar equation 2.3, the signal is weakened with increasing range and is also dependent on the targets shape, position and material. Hence, a target further away from the sensor will return a weaker signal than a similar target placed closer to the sensor. To account for this property of the radar, some sort of range compensation can be made. By making the amplitudes invariant to the range the amplitudes then represents the RCS of the target.

The idea is to compensate for this phenomenon where the compensation is dependent on the range. The proposed solution is to add or multiply this factor to all depth points in the output signal, $z(f, d)$. The proposed compensations are described by equations 2.21 and 2.22, where c is a constant which either reduces or increases the impact of the range, R, before the compensation.

$$\bar{z}(f, d) = z(f, d)(cR^x) \tag{2.21}$$

$$\bar{z}(f, d) = z(f, d) + (cR^x) \tag{2.22}$$

The exponent is either set to $x = 1$, $x = 2$ or $x = 4$ and determines the exponent of the range. Equation 2.21 for when $x = 4$ corresponds to the

theoretical dependence of the radar range to the target. This is in accordance with the radar equation. However, the effect of both multiplication and an exponent of 4 may result in to large compensation. Therefore, addition and smaller exponents could be used to find an appropriate compensation for the application. Since all equations are dependent on the range, the resulting signal will start to slope with a larger increase at larger ranges.

2.4.4 Correlation of peaks

The cross-correlation function is commonly used within statistics and signal processing to find relationships between two different time series signals. This can be applied to other types of signals with the main purpose of finding the best match at a certain lag, m. For discrete signals, $x(n)$ and $y(n)$, the cross-correlation, $R_{xy}(m)$, is defined according to equation 2.23. The correlation function is the sum of the product of corresponding points of the two signals for a certain m. One can view the operation as sliding one of the signals over the other, where the largest output is generated at a certain lag with the best match of the signals. In 2.23 the signal $y(n)$ is being slid over $x(n)$, where $*$ denotes the conjugate of $y(n)$ with m as the lag between the two. [22, 23]

$$R_{xy}(m) = \sum_{n=-\infty}^{\infty} x(n)y^*(n-m) \tag{2.23}$$

Cross-correlation can be used to correlate a detected peak with the consecutive frame. This could be used when the consecutive frame doesn't produce a detection, i.e. do not exceed the threshold. The result of the cross-correlation would be a prolonged detection of the target. The detected peak is cut from the frame output, $z(f, d)$, with a width of depth-indexes to ensure that the whole peak is cut since the width of the target may vary. The peak interval, $z_{cut}(f-1, d)$, is then correlated with the consecutive frame, $z(f, d)$, according to equation 2.24 only if no detection of the output threshold is made. To get a normalized correlation the mean of the two signals can be subtracted. A new threshold is introduced, μ_{corr}, and if the correlation of equation 2.24 exceeds this, the detection is prolonged.

$$R_{zz_{cut}}(f, m) = \sum_{d=-\infty}^{\infty} z(f, d)z^*_{cut}(f-1, d-m) \tag{2.24}$$

To prevent false detections, the lag of the new position of the target according to the correlation is compared with the previously detected position.

If the new position indicates an unreasonable large change, the detection is rejected and the cross-correlation is turned off. For example, if a target is detected at a distance of 3 meters would jump to 5 meters from one frame to another, it would be rejected since it would be a false detection.

Chapter 3
Method

This chapter will explain the methods used to evaluate the sensor, generate and evaluate concepts, how the data was acquired and lastly how the optimization of the detection algorithm was performed.

3.1 Sensor evaluation

The A111 sensor has been evaluated with respect to interference, beam angles and range. The evaluation aimed to gain knowledge of the sensor to determine its limitations and possibilities for a blind spot detection system. Properties evaluated was if the range is long enough, if interference will be a problem when using several sensors and how do the shape of the beam behave. All these initial tests were performed inside in a controlled setting without any disturbances such as moving objects or larger static objects.

3.1.1 Interference between two sensors

Any potential interference between sensors needs to be evaluated to determine if any processing or shielding is needed to minimize the potential effects. The potential interference was evaluated for both envelope and sparse service, with and without a lens. Two sensors were placed next to each other with a small angle of approximately five degrees, directing the sensors slightly away from each other.

To determine the type of the potential interference, shielding was placed between the sensors, this was only performed on the cases where interference occurred. This was done under the assumption that the interference could occur directly from one sensor to the other or from reflections of the other sensors transmitted pulses. The shield used was a metal sheet, which is a 20

centimeters wide and 30 centimeters long object made out of aluminium. This shielding was only performed for the envelope service.

3.1.2 Angles of the radar beam

One of the sensor properties which influence the number of sensors needed to cover the blind spot is the spread of the transmitted radar beam. One assumption made is that the beam shape is the same to the right as to the left due to symmetry, hence only the right side was measured and tested.

The evaluation of the H-plane was performed using both sparse and envelope service, with and without a lens. The angles were measured at 0.5, 1 and 1.5 meters. A schematic illustration of the setup as seen from above can be seen in figure 3.1. The sensor was placed at a height of 0.7 meters. A protractor was mounted with its center, i.e. $0°$, directly under the sensor. Lace was attached to the protractor.

A person was holding the lace on the left side, close to the body to enable the target to move constantly along the radius. The person started standing with the lace placed at $0°$ of the protractor and then moved $5°$ upwards along the radius until disappearing. Both the data from the radar and a video of the test person was recorded to attain correlation in time between different angles and the ability of detection. The radar data was replayed together with the video to visually determine at which angles when the target then disappeared. The resulting angles were documented.

Furthermore, the test of the H-plane was performed once more for both envelope and sparse service, but with a metal sheet as the target. The metal sheet was a 20 centimeters wide and 30 centimeters long made out of aluminium. This was done to evaluate how differences in reflectivity affect the detectability. The metal sheet was held with the flat side towards the sensor and with the lace on the left side at a distance of one meter. According to previously mentioned method, the sheet was moved along the radius until disappearing.

In addition to the evaluation of the H-plane, the E-plane was also investigated to evaluate the beam shape. The angles of the E-plane was determined by measuring the angles with a person as the target at a distance of 1.5 meters. This was mainly done to see if the E-plane follows the same behaviour as the H-plane. It was done for both the envelope and sparse service, with and without a lens and the method was the same as for the H-plane.

See tables 5.1 and 5.2 in the appendix for more detailed information of the settings used for the envelope and sparse service respectively during the evaluation.

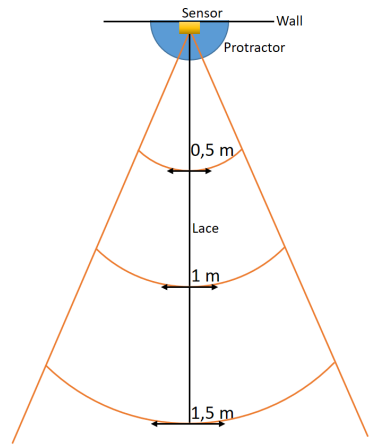

Figure 3.1: The setup of the test to evaluate the angles of the radar beam.

3.1.3 Range of detection

Another sensor property which is important for a blind spot detection system and is different for different radar sensors is the range. The range needs to be as long as possible to increase the time available to both process the data and notify the biker before an eventual accident.

Different settings and the effects of using a lens were evaluated for a biker and a pedestrian as targets to test how this would affect the range. Furthermore, the potential effects of different placements on the bike was evaluated. The sensor was mounted 0.7 meters above the floor. The target started close to the sensor and then slowly backed until no sign of detection could be made. The target then slowly moved towards the sensor again until clearly visible in the sensor data. A schematic image of the setup as seen from the side can be seen in figure 3.2.

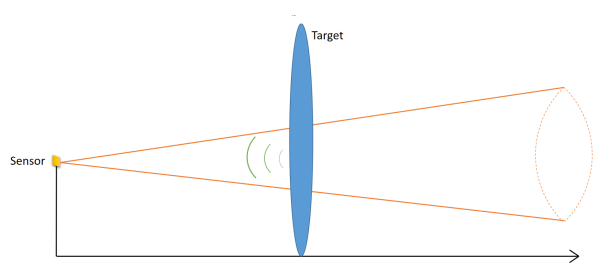

Figure 3.2: The setup of the test to evaluate the range of the radar beam.

The radar data was replayed to determine at which distance the target was visible and when the target disappeared. This was done to keep some consistency of how to determine when the target visually vanish. The results of the range were documented and then compared to the theoretical range.

By using the radar equation with approximations the theoretical range of five meters was obtained. The typical radar loop gain provided by Acconeer and the typical RCS of a pedestrian was provided by Yasugi et. al. [24] for a 79 GHz radar. This was done under the assumption that the SNR for a detection is around -10 dB.

Different targets and settings

It is needed for the blind spot detection system to be able to detect pedestrians and bikers. However, due to the shape and the permittivity of the target, the energy of the reflected signal may limit the range. The bike is made of metal which has high permittivity, but the shape of the bike may direct the radar away from the receiver reducing the received signal power. Hence, the evaluation was performed for a biker as well to determine if the bike would have any either positive or negative effect on the range.

Default settings were defined for both the envelope and sparse service when a pedestrian was the target. See table 5.3 and 5.4 in the appendix for more detailed information of the settings and in section 2.2 where the settings are briefly explained. To evaluate different settings, one parameter was altered at the time. The settings further evaluated of the envelope service was the profile, HWAAS and downsampling factor. For the sparse service, the settings evaluated was the profile, sweeps per frame and sampling mode. The number of missed frames and range was documented for all the different settings. From the result, ”optimal” settings were defined and tested and if these would outperform the previously default settings it would then used as new default settings. These ”optimal” settings can be seen in tables 5.5 and 5.6 in the appendix.

Sensor mounted under saddle

A simple test was performed to evaluate how the placement of the sensor may influence the range. Depending on the placement, the bike rack and mudguards may be detected reducing the transmitted and received energy of targets further away.

The effect of these potential reflectors was evaluated by holding the sensor under the saddle, directed backwards from the biker in parallel to the floor.

The settings used previously defined as default was used throughout the testing and the target was during these tests a pedestrian, see table 5.3 and 5.4 in the appendix.

3.2 Concept generation and evaluation

After the evaluation of the sensor property, different concepts was generated and then tested to find the final prototype configuration. To generate concepts suitable for the application the blind spot first needed to be defined. This definition will influence the number of sensors used in the first concepts. The concepts were then generated and evaluated according to both the measured range and angular coverage of the sensors.

3.2.1 Blind spot definition

The shape and placement of the blind spot of a car depend on the angling of the mirrors. If the side-mirrors are directed too much backwards, this will generate a blind spot close to the car, see illustration to the right in figure 3.3. If the side mirrors are directed too much towards the sides, this will generate a blind spot further away from the car, see illustration to the left in figure 3.3 [25]. The same principal is applicable on the blind spot system, i.e. there may be areas not covered by the senors if the number of sensors cannot cover the whole blind spot.

To evaluate and confirm the blind spot of the biker it was tested. The hypothesis was that the blind spot definition could be reduced since the biker usually turns the head to control the immediate surroundings before any sud-

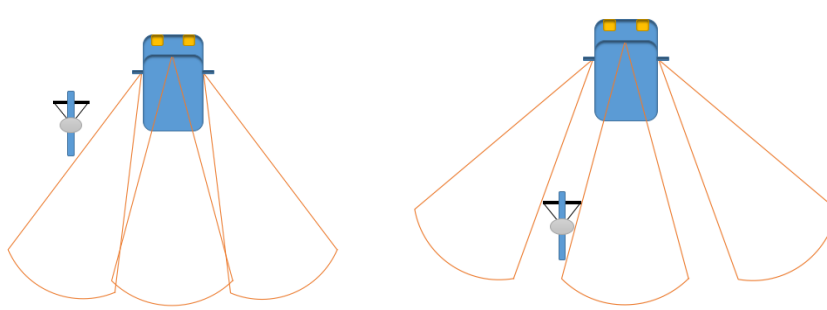

Figure 3.3: The blind spots generated by different angles of the mirrors in a car.

den change of direction. The motion of slightly turning the head to either side usually has no or small impact on the biker. Therefore, the visual blind spot may be redefined for the biker.

A target moved in the blind spot along the radius of three meters from the biker until the biker could visually detect the target. The angle when the target was said to be visible was determined using a protractor and lace attached on the bike. The target, a person, held the lace at three meters and slowly moved along the circle sector from the back towards the front. Due to the assumption of symmetry only the right side was tested. Two different persons, with different height, performed the test as the biker and due to the circumstances of Covid-19 there was limitations of performing a larger study. The test persons held their heads and their visual focus in different combinations to test the hypothesis and to test the comfortable blind spot, see the combinations in the list below;

1. The person had both the head and visual focus directed straight forward.
2. The person had the head directed straight forward but shifted the visual center comfortably to the side of the approaching target.
3. The person had comfortably shifted the head slightly to the side of the approaching target and the visual focus directed in the same direction as the head.
4. The person had again shifted the head slightly to the side of the target and the visual focus now directed towards the approaching target.

3.2.2 Concept generation

The results of the tests of the sensor specifications together with the new definition of the blind spot was used to generate several concepts. These concepts were then evaluated to determine the final concept which was intended to be the final prototype.

Due to the new definition of the blind spot and the angular coverage of one sensor, the number of sensors used was chosen to be three. The number of sensors should be as few as possible to reduce both the cost and size, however, it needs to be high enough to achieve the desired coverage. If three sensors should prove to be unreliable, new concepts with four sensors would then be needed to be generated and evaluated.

The placement of the sensors was either directly under the saddle or on the saddle-pole. These tests were intended to evaluate if the sensors would disturb

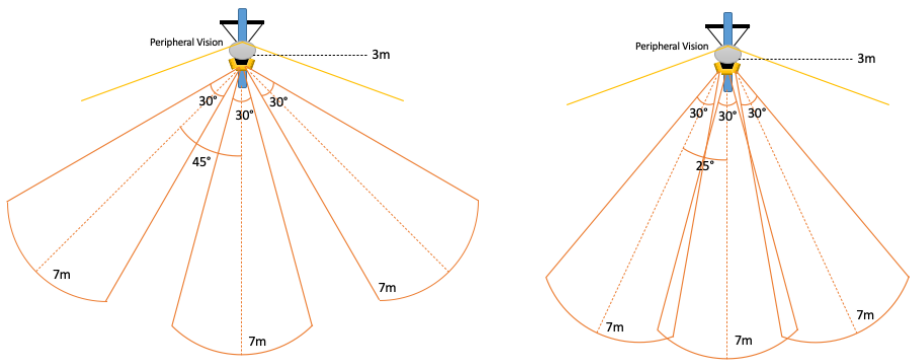

Figure 3.4: Two examples of the proposed concepts where the angles between the sensors are altered. To the left the angle is $45°$ and to the right the angle is $25°$.

the biker. The placement also affects how much reflections and disturbance there will be from both the bike and biker.

Furthermore, the concepts generated varied in both the angling between the sensors in the H-plane (from $45°$ to $25°$, with five degrees intervals) and in the angling in the E-plane (tilting five and ten degrees upwards, where zero is defined as parallel to the ground). Some explanatory illustrations of the angles between the sensors can be seen in figure 3.4, where the angle of $45°$ and $25°$ is demonstrated. The aim is to have angles which minimize the area not covered by the sensors to always detect the target.

Another difference between the concepts and previous tests was the usage of the lens holders designed by Acconeer. All concepts included the usage of lenses due to the increase in range, but not all was designed with the lens holder. Some concepts only had the lens attached over the sensor with one millimeter spacing, trying to replicate the D1 positioning from the lens holder. See definition of the D1 position in figure 2.4.

3.2.3 Concept evaluation

To evaluate the concepts different tests were conducted. Since the exploration tool is limited to one connection to the XB112 breakout board a new python script was developed. This script was intended to handle multiple sensors connected by USB and being enable to record and store data in h5-files. The evaluation was made using the sparse service and the settings used can be found in the table 5.6 in the appendix.

To begin with, the aim was to determine if the potential gap between the sensor fields could be acceptable. A gap may not affect the ability to detect the targets due to the target's shapes and elongation.

Two separate tests was conducted to evaluate the ability to detect the target along different radii and different paths in parallel with the center of the sensor-setup. Since the number of sensors was three, the tests were only performed on one side of the bike due to the assumption of symmetry in the sensor setup. The tests can be seen described in the list below. The sensors in the generated concepts were angled differently in both the E-plane and H-plane. Hence, the two tests were performed several times for every change of any angle.

1. Firstly, the target moved along radii at the distances of 3, 5 and 6.5 meters, see figure 3.5 for a visual overview. The target was a pedestrian who moved along the radius holding a lace. A protractor was used to read the angles. A video was recorded showing how the lace moved along the protractor as the target moved in the radius. The video and the sensor data was replayed to document the angles. The angle when the target was no longer visually detectable by the center sensor, when the target became detectable by the right sensor and when the target was no longer detectable by the right sensor was documented.

2. Secondly, the target moved in parallel with predefined distances of 0.5, 1, 1.5, 2, and lastly 2.5 meters from the center of the middle sensor. See figure 3.6 for an overview of the test. Both a pedestrian and a biker was used as targets. The recordings from the sensors were then replayed to determine the distances of when the target was barely visible and visible. This was made independently by two individuals and then averaged to make the results less subjective.

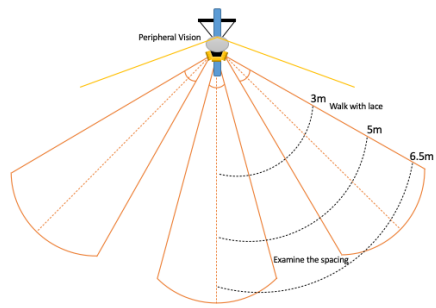

Figure 3.5: Overview of the test of the spacing between the sensors seen from above. The proposed radii are marked and demonstrates how the target moves.

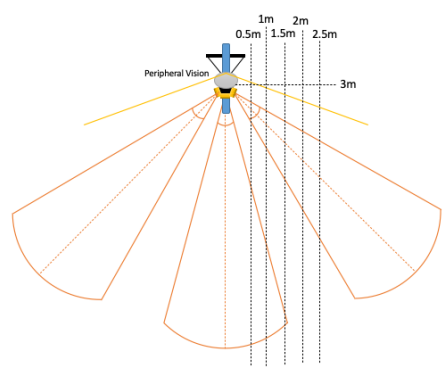

Figure 3.6: Overview of the test of the spacing between the sensors seen from above. The proposed distances from the defined center are marked and demonstrates how the target moves.

Further evaluation of settings

The aspect of different settings affecting the range of the sensors was also further evaluated. Tests were performed to find the final optimal settings for the purpose of a blind spot detection system. The evaluation was based on the visual inspection of raw data.

The downsampling factor was chosen to be 4 during all combinations to reduce the number of missed frames with the number of sweeps per frame as high as possible. The three combinations which were tested can be seen in table 3.1.

During this evaluation, the angles were set to 30° between the sensors and no angling in the E-plane. Lens holders were also used on all sensors. The target was a pedestrian who moved in parallel with the center of the middle sensor, at the distances 0.5, 1 and 1.5 meters. See figure 3.6 for an overview of the test.

The recordings of the raw data were evaluated by replaying the data to determine the distances when the target was barely visible and visible. The distances were determined independently by two individuals to make the results less subjective. The final evaluation was then made by comparing the changes between the range determined.

Table 3.1: The different settings tested to find the final optimal settings of the sensors for the application. Target was a pedestrian and biker in test 1. For the rest of the tests, only a pedestrian was the target.

	Profile	**Sweeps per frame**	**Range (m)**
Test 1	4	32	0.5-7 for all
Test 2	4	42	0.5-5 for all
Test 3	3	42	0.5-5 for all

3.3 Data acquisition

To develop and evaluate a system for a blind spot system for eBikes, the final concept was used to attain recordings of raw data used to train and test different algorithms.

The final setup consisted of three sensors with a 30° angle in the H-plane, all with a hyperbolic lens in a lens holder. The sensors were mounted directly under the saddle. Furthermore, the sensors were directed backwards in parallel with the ground, i.e. no angle in the E-plane. See figure 3.7 for a visual demonstration of the final setup. Sparse service was used and the settings can

be seen in the table 5.6 in the appendix which is the final set of sensor specific settings. During the generation of data, a biker was used as the target. The recordings were also captured with a GoPro MAX 360° camera to be able to later attain the ground truth.

Figure 3.7: The final setup of the sensors on the biker. The left image shows the setup without lens holder to more clearly demonstrate the placement of the sensors. The other image shows the setup with lens holder.

3.3.1 Recording of sensor data

A generated Python script that stored every frame and the settings was used. In the script, the settings that have to be defined before a recording can be altered for each sensor individually. When the recording starts, all sensors starts and samples simultaneously. The sensors were attached by the USB-ports to a Raspberry Pi. When the Raspberry Pi reboots or when power is connected, a shell script will launch which runs the Python script. A breadboard is connected to the GPIO-pins of the Raspberry Pi.

On the breadboard, two buttons and two diodes were attached. One was green and one was red and they were used to indicate the status of the script, i.e. if ready to start recording of data or if it was recording. In addition to this, the two buttons were used to start and stop the recording.

After stopping the recording, all frames and different settings could be saved into a file in H5-format. Evaluation of the recorded data could then be made by replaying the raw data with post-processing and the eventual recorded video.

3.3.2 User cases

The sparse service data acquisition was performed for three user cases, UC, designed with an increase of surrounding disturbances for every case. The scenes were designed to mimic previous tests and real life scenarios of a target approching in the blind spot. Together with this, the moving patterns intend to both investigate the sensor gap between the sensors, which is why targets cross the sensor paths, as well as the trackability. UC 1 intends to be the easiest with no disturbance from movements of the biker or in the surroundings to minimize the noise. During UC 2 and 3 the bike is moving. UC 2 holds no disturbances from the surroundings just eventual noise from the movement. The last UC intends to reflect real biking scenarios with movements and disturbances present. The aim was to evaluate the effects of the noise on the data and how to minimize the different sources of noise. The three recording sets were performed twice, once to generate data for training and once to generate data for testing.

For UC 1, the recordings were made on a gravel football court, since an open court holds no potential disturbances. To gain depth resolution in the recorded video from the 360-camera, markings were made in the gravel according to the orange markings in figure 3.8. Hence, the markings made followed the previously tested shape of the beam in the H-plane, i.e. the shape of a circle sector with 30° spread and a length of seven meters, making it possible to distinguish the true range to the target in the video playback. The recordings were then made according to figure 3.8 resulting in a set consisting of eleven training and eleven testing recordings. These moving patterns intend to capture typical movements of a target approaching in the blind spot at different positions. The video recorded scene can be visualized in figure 3.9 where one can see the markings in the gravel and a target approaching the biker which is standing still.

During UC 2, the recordings were made on an empty parking lot since the location has no potential disturbances. To gain depth resolution in the recorded video, a lace was attached to the end of the bike which had markings every meter from one to seven meters. On the bicycle rack, 20 centimeters long rods were placed to indicate the edges of the sensors field, i.e. marking the 30° angle between the center of each sensor. A schematic overview of the placements of the rods and the rope can be seen in figure 3.10. The movements during each recording were according to figure 3.11, resulting in a set of both nine training and testing recordings. The movements should represent both the recordings of UC 1 and some real-life situations for when a target is appearing or cruising in the blind spot. The video recording of the scene is

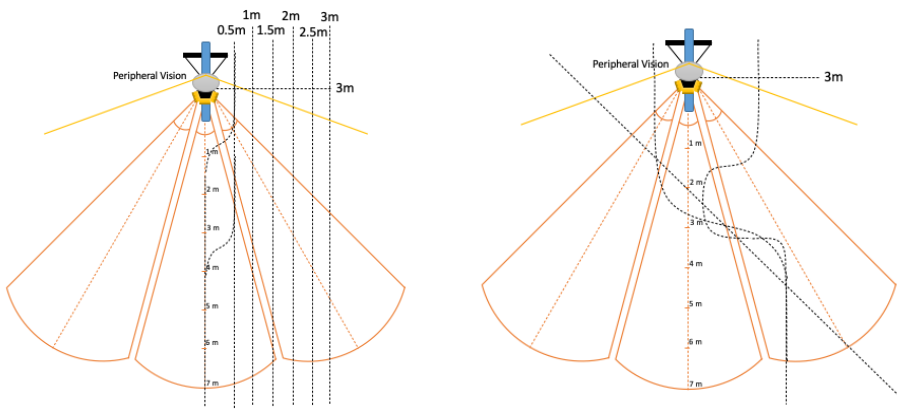

Figure 3.8: An overview of the movements recorded during UC 1. The dotted lines indicates the paths of the target, resulting in eleven different paths and recordings for this UC.

Figure 3.9: Images from UC 1 showing the setup during the data acquisition. The target is approaching to the left and also from the center.

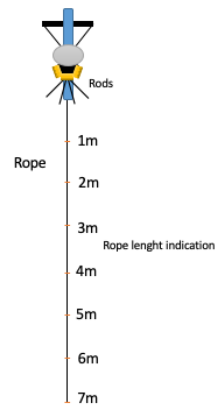

Figure 3.10: An overview of the setup to gain depth resolution in the recorded video during UC 2.

captured in the figure 3.12 for two of the recordings for this UC.

UC 3 consisted of longer recordings, where the biker and the target went around an area with trees, bushes, cars, pedestrians, bikers etc. The target cruised within the blind spot at different ranges and from left to right during approximately two minutes. To avoid any potential accidents, the lace was removed since it could disturb or get caught in other objects. However, the rods were still used according to figure 3.10 to indicate the edges of the sensor field. Two different routes were recorded twice each, to generate two sets of training and test data. Images capturing the final UC can be seen in figure 3.13 where the top two images is of the first route and the bottom two is of the second.

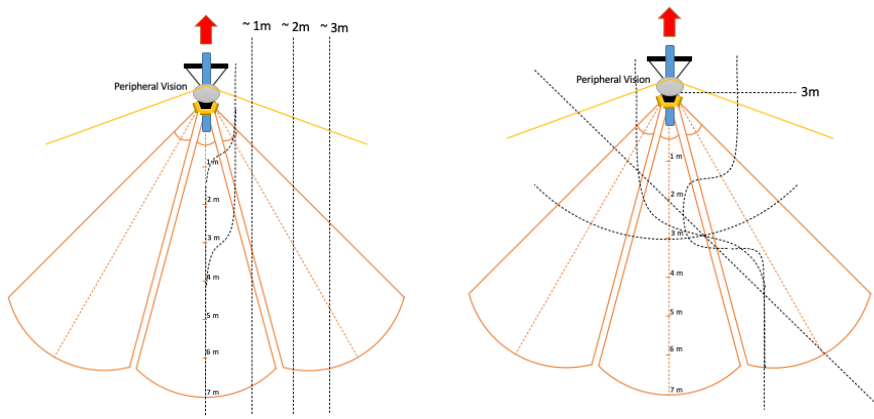

Figure 3.11: An overview of the movements recorded during UC 2. The dotted lines indicates the paths of the target, resulting in eleven different paths and recordings for this UC.

Figure 3.12: Images from UC 2 showing the setup during the data acquisition. Target cruising and approaching in the blind spot where the biker now moves as well.

Figure 3.13: Images from UC 3 showing the setup during the data acquisition. Target cruising and approaching in the blind spot of the two routes, top two images is the first route and the two bottom is the second.

3.3.3 Annotation of ground truth data for validation

To evaluate the results from the implementation of potential improvements in the processing, sets of validation data was annotated. The validation data can be seen as the ground truth to the expected output from the processing.

All UC were recorded using a GoPro MAX-camera that captures a 360-degree video with a frame rate of 30 Hz. The video was first scaled into an MP4-video in two dimensions and then cropped to start at the exact moment when the recording started.

A Python script was generated which replays the MP4-video with the possibility to pause and then step forward 0.5 seconds at the time. During the replay of the video, manual annotation of each sensor field was made. When the target was within a specific sensor's field of view a key was pressed to get the exact frame index where the target should be detected. The key was also pressed when the target left the field of view. Intervals, where the target should be detectable for each sensor, was generated and expressed in frame indexes. The generated ground truth for each sensor were then saved in a vector in an H5-file.

3.4 Detector optimization

The post-processing used affects how well the system can detect the desired targets. To optimize the post-processing's ability to detect the targets the optimal parameters of the algorithms needed to be found.

3.4.1 Accuracy

The comparison between the output of the processing of the training set and the ground truth was made to determine the number of true positives, false positives, true negatives and false negatives. If the target was present or not in each sensor field, i.e. yes or no, was compared and not the distance to the target. The ground truth data holds whether the output should be yes or no. If the system then makes a detection when a detection should be made according to the ground truth it is a true positive, TP. Furthermore, TN are the true negatives, which is when the system does not make any detection and should not have made any detections. FP is the measure of false positives, i.e. the system makes a detection when a detection should not be made. Lastly, FN stands for false negative, i.e. the system does not make any detection when a detection should be made.

The accuracy was maximized during training to optimize the parameters of the chosen post-processing. The accuracy range between zero and one, where one means 100% correct measurements compared to the ground truth. Using the TP, TN, FP and FN the accuracy can be calculated according to equation 3.1. The resulting accuracies for each processing were then evaluated. This was done to find the best processing since the accuracy holds information regarding both the part of missed detections (FN) and the part of false detections (FP), which is favourable since these parts should be minimized.

$$\text{Accuracy} = \frac{TP + TN}{TP + FP + TN + FN} \tag{3.1}$$

3.4.2 Optimization of detection algorithms

An optimization algorithm was used to speed up the process of finding the best settings of the processing since the parameters influenced each other. The algorithm chosen was designed to maximize the mean accuracy of the chosen UC and is called the Nelder-Mead algorithm. The algorithm was chosen due to its simplicity.

Firstly, the optimal sparse presence detection settings which maximised the accuracy for each UC were found using the Nelder-Mead algorithm. If the accuracy of UC 1 would be over 85%, then only UC 2 and 3 would be used in all further evaluation. Since UC 1 was recorded during optimal circumstances it is hard to improve the accuracy without overtraining on a situation without noise. Therefore, 85% is chosen as the initial guideline and breaking point to decide when to stop optimizing on this easiest UC. This together with the replay of the data was used to show the use of the sensor and the raw data. Furthermore, the Nelder-Mead algorithm was then used again to find the optimal settings for the combination of UC 2 and 3. The settings which result in the highest accuracy for both UC was said to be the most generalized optimal settings on the training data set.

The different types of added post-processing evaluated can be seen in table 3.2 together with the parameters which was trained to optimize the accuracy. Integer parameters such as $N_{average}$, N_G, N_{CFAR} etc were set manually and the rest optimized using the Nelder-Mead algorithm. After all types of processing had been optimized the ones which increased the accuracy the most was combined and evaluated further. The final resulting accuracy of the best combination together with visual verification of the output, was chosen as the final processing.

Table 3.2: The different types of processing evaluated using the Nelder-Mead algorithm. The design parameters of the algorithm are also listed.

Processing	**Design parameters**
Sparse presence detection settings	$\boldsymbol{\tau_{intra}}$ $\boldsymbol{f_{c(slow)}}$ $\boldsymbol{f_{c(fast)}}$ $\boldsymbol{\tau_{inter}}$ $\boldsymbol{w_{intra}}$ $\boldsymbol{\tau_{output}}$ $\boldsymbol{v_{threshold}}$
Compensation of range For equations 2.21 & 2.22 when $x = 1, 2, 4$	$\boldsymbol{v_{threshold}}$ Range compensation factor, C
CFAR	$\boldsymbol{\mu_{CFAR}}$ $\boldsymbol{\tau_{intra}}$ $\boldsymbol{\tau_{output}}$
Correlation of peaks	$\boldsymbol{v_{threshold}}$ $\boldsymbol{\tau_{intra}}$ $\boldsymbol{\mu_{corr}}$
CFAR + Correlation of peaks	$\boldsymbol{\mu_{CFAR}}$ $\boldsymbol{\tau_{intra}}$ $\boldsymbol{\mu_{corr}}$
CFAR + Correlation of peaks Different settings for side sensors	$\boldsymbol{\mu_{CFAR}}$ $\boldsymbol{\tau_{intra}}$ $\boldsymbol{\mu_{corr}}$

3.4.3 Validation of detection performance

The chosen processing was then controlled, by using the test data sets, to verify good generalization and potentially reject the possibility of overtraining. In addition to accuracy, the sensitivity and specificity was also calculated from the TP, TN, FP and FN according to equations 3.2 and 3.3. These metrics was calculated to say whether the obtained solution is optimized to correctly generate a true detection and to correctly say whether no target is present in the blind spot.

$$Sensitivity = \frac{TP}{TP + FN} \tag{3.2}$$

$$Specificity = \frac{TN}{TN + FP} \tag{3.3}$$

Chapter 4
Results

The following sections holds the results from the sensor evaluation, the concept generation and evaluation, the data acquisition and lastly the optimization of the blind spot detector.

4.1 Sensor evaluation

4.1.1 Interference between two sensors

Interference was visible when using the envelope service, see figure 4.1, while for the sparse service it was not, see figure 4.2. The interference could be seen as quick peaks visible during one to two frames in the frame output over time for envelope. The interference could be avoided by placing the metal shield between the sensors. The recorded data history of sparse is harder to interpret since it shows the mean of each depth rather than the history of the raw frames. It could not be seen for the playback of data and within frames and since no clear disturbance in the raw data frames could be seen, shielding was not tested. Usage of a lens was also tested and did not influence the results for either envelope or sparse.

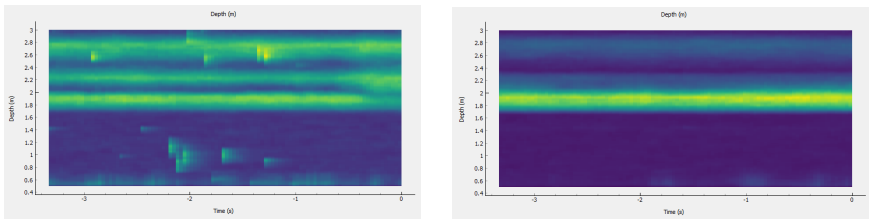

Figure 4.1: The results showing interference when using the envelope service without a lens and when using a shield. The left image show the interference without lens. The right image shows the results of adding a shield. Images are taken from the GUI provided by Acconeer.

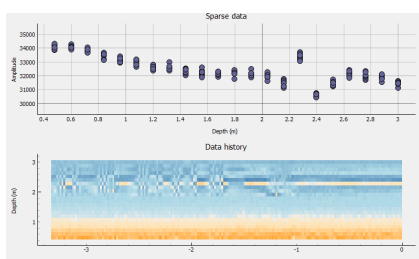

Figure 4.2: The results showing no clear interference when using the sparse service without lens. Images are taken from the GUI provided by Acconeer.

4.1.2 Angles of the radar beam

The results of the measurements of the H- and E-plane can be seen in the tables below for both sparse and envelope service, both with and without a lens. H-plane measurements for envelope service and sparse service can be seen in table 4.1. The results for the E-plane can be seen for both sparse and envelope service in table 4.2. The angles are defined with zero degrees in the middle of the sensor center and increasing angles towards the side. The angles documented are the angles when the target becomes undetectable at different radii.

Table 4.1: The measured angles in the H-plane, for several radii, when using the envelope and sparse service, both with and without a lens. The results when changing the target is also showed.

H-plane - Envelope				
	0.5 m	**1 m**	**1.5 m**	**Metal 1 m**
No lens	50°	35°	35°	40°
Lens	25°	15°	15°	20°
H-plane - Sparse				
	0.5 m	**1 m**	**1.5 m**	**Metal 1 m**
No lens	55°	40°	40°	40°
Lens	25°	20°	15°	20°

Table 4.2: The measured angles in the E-plane using the envelope and sparse service at the radius of 1.5 meters from the sensor.

E-plane		
	Envelope	**Sparse**
No lens	15°	20°
Lens	15°	15°

The width of both the H- and E-plane reduces as the range increases resulting in a beam shape which is not coherent, i.e. the cone shape is not consistent and narrows down as the distance increases resulting in a more teardrop shape. This applies to both envelope and sparse service, with and without lens. The strongest reflectance was attained when target was directly in front of the radar sensor, this behaviour was seen for both sparse and envelope service. The metal gave the strongest signal return of the different targets.

The measured angles when using sparse service is approximately five degrees larger than when using envelope service. Hence, one can see a tendency of the sparse service outperforming the envelope service when it comes to having a consistent radar beam shape.

4.1.3 Range of detection

Range measurements with different targets

The results from the range measurements when the target was a pedestrian can be seen in table 4.3 for both the envelope and sparse service, with and without a lens. Both the range of the detection, i.e. when the target becomes visible, and the missed frame ratio was documented. The range needs to be as large as possible to increase the time to notify the biker.

The results shows that the usage of lens drastically increases the range of detection for both the sparse and envelope service. It can also be seen that profile 4 results in a larger range for both services. Furthermore, it was found that sampling mode B and a high sweeps-per-frame rate is desirable to receive a good detectability during increased ranges. Moreover, larger downsampling seems to reduce the number of missed frames and increase the range of detectability.

Another notation is that the number of missed frames differs when comparing the different services, with high values for the envelope service and small to non-existing missed frames for the sparse service.

Finally, the range is larger in general when using the sparse service. However, the measured range was shorter than the theoretical range. The calculated range determined was 5 meters using the approximations. However, the measured range was in general only up to 2 meter without lens. Lens did increase the range by approximately 3-4 meters for both envelope and sparse.

The effects on the range from when changing the target can be seen for both the sparse and envelope service in table 4.4. The range of detection with and without a lens can be seen. Small differences in the range can be seen between the different targets when using the default settings, but when using the ”optimal” settings the range is unchanged. However, the range of the sparse service is superior to the envelope service.

Since the sparse service showed to be superior to the envelope service in regards of the range, which is an important factor of the proposed application, the decision was made to discard the envelope service. Hence, only the sparse service was used in the testing and evaluation which followed. The use of lens from here on is motivated by the large range gain. The increased range is better

Table 4.3: The measured ranges and the missed frame ratio when using different settings of both envelope and sparse service, with and without a lens. Settings started with the default and then the default together with the changed stated parameter. The target was a pedestrian.

Envelope						
		Default	**Profile 4**	**HWAAS 63**	**Downsampling 1**	**"Optimal"**
No lens	**Range**	2 m	2 m	2.1 m	2 m	2.1 m
	Missed frames	427/890	408/960	495/633	252/253	0/1607
Lens	**Range**	4.2 m	4.6 m	4.5 m	3.8 m	5 m
	Missed frames	443/930	502/1178	728/928	416/417	627/1174
Sparse						
		Default	**Profile 4**	**8 sweeps/frame**	**Sampling mode A**	**"Optimal"**
No lens	**Range**	2.2 m	2.6 m	2.2 m	1.8 m	3 m
	Missed frames	0/2952	0/3549	0/2731	1/2745	0/1878
Lens	**Range**	6.6 m	6.9 m	6.2 m	4 m	6.9 m
	Missed frames	0/3705	0/3145	0/3793	0/4177	0/2557

Table 4.4: The measured ranges when using different settings of the envelope and sparse service, with and without a lens. Settings started with the default and then the "optimal" parameter obtained before. The target was a biker.

Envelope		
	Default	**"Optimal"**
No lens	1.9 m	2.4 m
Lens	4 m	5 m
Sparse		
	Default	**"Optimal"**
No lens	3 m	3.1 m
Lens	5.5 m	6.9 m

than the drawback of decreased angular coverage which can be compensated with using more sensors.

Sensor mounted under saddle

The results of placing the sensor under the saddle when using the sparse service used can be seen in figure 4.3. To the left the pedestrian stands at the distance of 2.5 meters which can be seen due to the large variance of the sweeps. To the right the target had moved and was no longer present. However, a drop in amplitude at 0.4 meters can be seen. This could be seen as small variations when the target was present and it was more clearly when the target was not present.

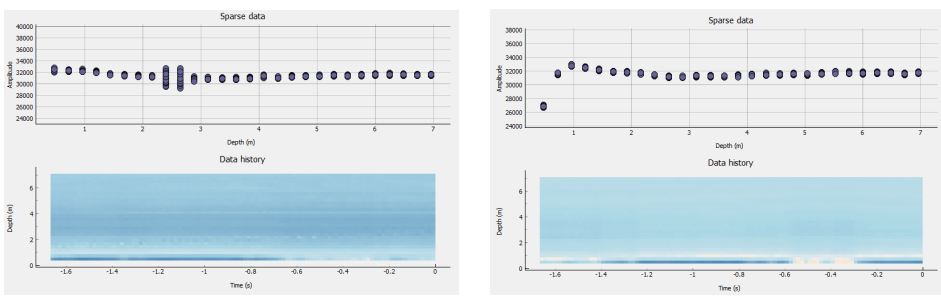

Figure 4.3: Result when using the sparse service. Pedestrian is present to the left and is not present to the right. Image is taken from the GUI provided by Acconeer.

The presence present at 0.4 meters was concluded to be the bike itself, i.e. the bicycle rack and mudguard. Hence, the range preset in the setting of the sparse service was set to start at a minimum of 0.5 meters to exclude the presence of the bike.

4.2 Concept generation and evaluation

4.2.1 Blind spot definition

The results from the evaluation of the blind spot can be seen in table 4.5. A similar result was given for both test persons in all four tests. The result of test one is worse than the theoretical coverage. It covers approximately 120° compared to the peripheral vision which covers approximately 80° to one side. However, test two and three showed that a slight tilting of the head

or shift in the eyes reduces the blind spot from 120° to approximately 50-55°. Combining the tilting of the head and shift of the eyes according to the fourth test resulted in an angle of 10-15°.

Table 4.5: The resulting angles which define the blind spot when directing the head and eyes according to the method for two test persons. The angles are defined with zero degrees as straight backwards from the biker.

	Test person 1	**Test person 2**
1	120°	120°
2	55°	50°
3	50°	55°
4	10°	15°

The requirement of tilting the head or shifting the eyes was added to the definition of the blind spot of the biker, reducing the total angular coverage needed from 160° to 100° directly backwards. See figure 4.4 for a schematic image of the definition of the bikers blind spot as seen from above. The biker can easily shift the head or eyes slightly to each side before turning and then entrust the sensor package to cover the rest of the blind spot. However, it is desirable, if possible, to cover the 120° angular range for the inattentive user. However, because of the reduce in costs, amount of data and computational complexity the number of three sensors is used initially to cover as much as possible of the full 240°, but with at least a 100° coverage.

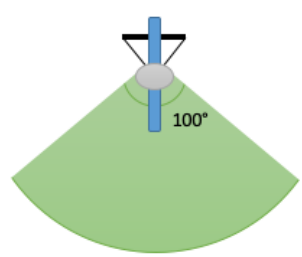

Figure 4.4: The definition of the biker blind spot.

4.2.2 Concept generation

When testing placement of the sensors it was found that the leg of the biker would cover the side sensors of all concepts when the placement was on the saddle pole. By placing the sensor directly on the saddle this effect was removed. Hence, the placement was decided to be under the saddle and not on the saddle pole.

The further concept generation was therefore reduced to only changing the angles in the E- and H-plane and testing the lens holder.

4.2.3 Concept evaluation

The result of the evaluation of the potential overlap or gap between the three sensors, at different angles in the H-plane, can be seen in table 4.6. In the appendix, more elaborate results can be found in table 5.7. The range when both biker and pedestrian as the target for different angles in the H-plane can be seen in the appendix in tables 5.10 and 5.11. All tests were conducted with lenses but without any lens holders.

The results show that the sensor underperforms compared to the specifications. For a closer range, the angular coverage is larger, and for a larger range, the angular coverage is smaller. Consequently, the sensor gap was greater at larger ranges. However, it was shown that an angle of $35°$ had no sensor gap at 3 meters. A small sensor gap could be seen at 3 meters during $30°$ but was not present at $25°$. This indicates that some small error may have occurred and no sensor gap should be present for $30°$. It can be seen that at the distance of 6.5 meters the sensor has difficulties detecting the target at the defined circle sector.

Furthermore, the gap seems to decrease as the angle decrease between the sensors as predicted. However, the gap doesn't decrease constantly. Moreover, there seems to be some sort of randomness, e.g. in table 4.6 the gaps of the $30°$-setup increase for both the radius of 3 and 5 meters after only decrease between the other angles.

The second part of the evaluation was made to determine the ranges of where different targets could be detected and tracked. Again, the results showed that the shape of the beam was not coniform, see figure 4.5. It can be seen that the larger the sensor angling was the larger the sensor gap became. Furthermore, the center sensor is very limited to any side of the middle. This can be seen for distances larger than 1 meter since the target is seldom visible. For the side sensors, the larger the angle between the sensors, the later the target becomes visible. Furthermore, during the visual determination of range, it

Table 4.6: The sensor gap present at different angles between the sensors at several radii, i.e. 3, 5 and 6.5 meters. Target was a pedestrian and the measurements were made for different angles in the H-plane.

	45°	**40°**	**35°**	**30°**	**25°**
3 m	10°	5°	0°	5°	0°
5 m	45°	30°	25°	30°	10°
6.5 m	40°	45°	30°	20°	-

was noted there was no apparent sensor gap between the center and side sensor. The potential sensor gaps were all small enough for the target to always be detected by one of the sensors, making it possible to always track of the target.

Some variation could be seen in the results. The placement of the center sensor was constant during all different angles of the side sensors. Hence, the expected range would be consistent for the center sensor during all tests. However, the range and detectability varied between the tests and was not consistent as predicted. Therefore the decision was made to only use the results as guidelines in combination with the theory to choose the final concept.

The angle of 30° was chosen and used as final concept for the following evaluation since the configuration showed to cover the most of the blind spot without any prominent sensor gap. Hence, concepts consisting of four sensors was not evaluated since the results showed to cover the wished area of the blind spot.

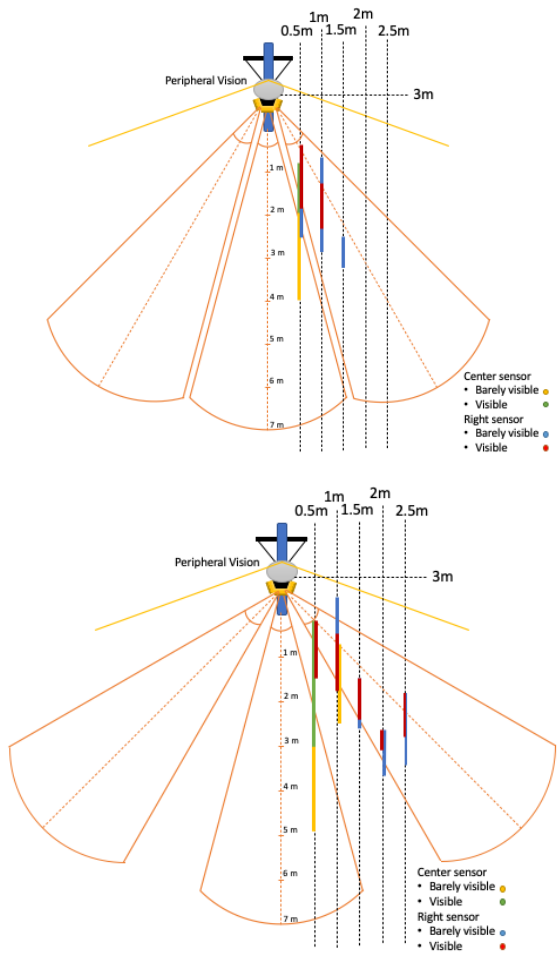

Figure 4.5: Visualization of the intervals where the target is visible and barely visible for each sensor. The angles between the sensors are 30° and 45° respectively.

Lens holder

The effect of using a lens holder was evaluated since the range of the sensor setup had underperformed compared to the expectations. The results of the same evaluation tests as the previous part, but with lens holder, can be seen in table 4.7 where the generated sensor gap is documented. More detailed results can be seen in the appendix in tables 5.8 and 5.9.

Some variation could be seen in the results, i.e. when comparing the results from two data recordings at the same distance and the same type of target a difference of 1-0.5 meters in range could be seen. However, the range was improved by at least one meter with the lens holder for both targets.

Furthermore, the angles that each sensor covers were more consistent than previous results. This can be seen comparing table 4.6 with table 4.7 and indicates a more stable positioning of the lens.

The lens highly affects the direction and shape of the beam and therefore its placement needs to be exactly correct. Hence, since the results were more stable, the decision was made to use the lens holders with the hyperbolic lens placed in the D1 position in the final concept.

Table 4.7: The sensor gap present at several radii, i.e. 3, 5 and 6.5 meters, when using lens holder and 30° angle between the sensors. Target was a pedestrian and the measurements were made twice.

	1	**2**
3 m	0°	5°
5 m	10°	10°
6.5 m	15°	15°

E-plane evaluation

The results from evaluating different angles in the E-plane can be seen in table 5.12. The angles tested was 5° and 10° tilting upwards from being parallel with the ground. Again, the targets tested was both a pedestrian and a biker.

When comparing the results from the different angles in the E-plane with the results when using no angle, it can be seen that the angling worsens the range of the center sensor. The range when the target was barely visible decreases from 6 meters to 5.5 meters in general. However, the results showed that the range of the side sensors was not affected by the change of angles in the E-plane.

Since the angles worsened the range of the center sensor and did not affect the others noticeably, the decision was made to not change the angling in the

E-plane.

Further evaluation of settings

The results from testing the three different settings can be seen in table 5.13. The results showed no radical improvement of the range for any of the changed settings. The usage of profile 3 reduced the range at 1 meter from the middle of the center sensor from approximately 4 to 3.5 meters.

According to the theory (Sec 2.4) and the result, it is favourable to maximize the number of sweeps per frame to be able to capture fast movements in the intra-frame part of the sparse service. To generate a robust estimation of the variance the number of sweeps per frame needs to be as large as possible. The maximal number of sweeps possible without getting any missed frames was showed to be 42 when using a downsampling factor 4 and profile 4. The results showed no improvement when using 42 sweeps per frame comparing to 32. The decision was made to use fewer sweeps per frame to reduce the amount of data.

The final sparse service settings obtained from the initial evaluation is visualized in table 4.8.

Table 4.8: The final settings obtained for the sparse service.

Final settings for sparse service	
Range interval (m)	0.5 - 7.0
Profile	4
Update rate (Hz)	60
Sweeps per frame (Hz)	32
Sampling mode	B
Repetition mode	Sensor driven
Downsampling factor	4
HW acceleration average samples	63
Gain	0.5

4.3 Data acquisition

The data acquisition and the ground truth annotation was made without any inconveniences. The number of data sets acquired for each UC can be seen in table 4.9. Each set consists of the data, the MP4-video and the validation file generated for both the train and test recording of the same movement. UC 1 and 2 holds many recordings of approximately 10 seconds and UC 3 holds

two minutes long recordings which are fewer. This results in the total amount of data for each UC to be close to equal even if it is distributed differently.

Table 4.9: The number of training, testing, validation and videos acquired from the data acquisition of the three UC.

	Training	**Testing**	**Validation**	**Videos**
UC 1	11	11	22	22
UC 2	9	9	18	18
UC 3	2	2	4	4

4.4 Detector optimization

4.4.1 Optimization of detection algorithms

Optimizing sparse presence detection parameters

The results given for UC 1, when optimizing the parameters of the Acconeer sparse presence detection algorithm, can be seen in table 4.10. During the optimization of the parameters for UC 1 using the Nelder-Mead algorithm, a clear tendency could be seen to tune the to $w_{intra} = 1$. By setting w_{intra} to 1, the inter-frame part becomes deactivated. Hence, w_{intra} was manually set to 1, and all parameters connected to the inter-frame part removed from the training. The result for optimizing the remaining parameters is shown in the table 4.11 where one can see that the algorithm converged to a set of settings adapted for the UC 1 training-set which yielded an accuracy of 0.8944.

In addition to these parameters, different $N_{average}$ for the depth running average filter were tested for UC 1. The filter with a $N_{average} = 1$, i.e. no filter, gave an accuracy of 0.8944. For $N_{average} = 2$ an accuracy of 0.8964 was obtained and for $N_{average} = 3$ gave the accuracy of 0.8964. Lastly, $N_{average} = 4$ resulted in an accuracy of 0.8956. The lack of a large increase in accuracy was the motivation to continue with no depth filter in the evaluation that followed, i.e. $N_{average} = 1$.

Optimizing the resulting parameters on the other UC gave the results which can be seen in table 4.11. The parameters do not vary much between each UC, except for $v_{threshold}$ which is higher for UC 2 and 3. As can be seen in the results, the accuracy is over 85% for all sets of training data. It becomes clear that UC 3 is the most difficult with a performance of 0.8663. Since the accuracy for UC 1 is over 89%, the decision was made to not train the parameters for future processing alternatives on UC 1. The training was then

Table 4.10: Final convergence of the Nelder-Mead minimization algorithm performed on the sparse presence detection parameters for UC one. Presented are the parameters which yielded the given accuracy.

Processing settings	
	UC 1
τ_{intra}	0.14
$f_{c(slow)}$	0.21
$f_{c(fast)}$	19.02
τ_{inter}	0.45
w_{intra}	0.99
τ_{output}	0.49
$v_{threshold}$	1.60
Accuracy	0.8704

Table 4.11: The final settings and accuracy generated from the optimization sparse presence detection using the Nelder-Mead algorithm. The optimization was made using training data sets of UC 1, 2 and 3, and lastly a combination of UC 2 and 3.

Processing settings				
	UC 1	**UC 2**	**UC 3**	**UC 2&3**
τ_{intra}	0.14	0.15	0.15	0.16
τ_{output}	0.16	0.15	0.15	0.15
$v_{threshold}$	1.31	1.62	1.62	1.60
Accuracy	0.8944	0.8932	0.8663	0.8887

focused to minimize the effects of different types of noise and disturbances which are present in UC 2 and 3.

Compensation of range

When applying range compensation to the processing, the results of the Nelder-Mead algorithm showed no or very small improvement when comparing the results with no range compensation made. The results from the range compensation can be seen in table 4.12 and 4.13. Using $x = 2$ showed no improvement. The decision was made to not test $x = 4$ even if this is the correct compensation according to the theory. The $x = 4$ would have given even larger changes at further ranges than $x = 2$ and hence worsened the result. The only compensation which did improve the accuracy was the compensation

Table 4.12: The final parameters and accuracy generated from the optimization of range compensation using the Nelder-Mead algorithm. The optimization was made using UC 2 and 3. The range compensation presented was founded on equation 2.21 when $x = 1, 2$.

Compensation of range				
	$x = 1$		$x = 2$	
	UC 2	**UC 3**	**UC 2**	**UC 3**
$v_{threshold}$	0.17	0.17	1.11	1.02
Range compensation factor, C	0.26	0.16	0.19	0.10
Accuracy	0.8713	0.8438	0.8496	0.7673

Table 4.13: The final parameters and accuracy generated from the optimization of range compensation using the Nelder-Mead algorithm. The optimization was made using UC 2 and 3. The range compensation presented was founded on equation 2.22 when $x = 1, 2$.

Compensation of range				
	x = 1		**x = 2**	
	UC 2	**UC 3**	**UC 2**	**UC 3**
$v_{threshold}$	1.62	1.54	2.18	2.15
Range compensation factor, C	0.2	0.22	0.19	0.19
Accuracy	0.8955	0.8670	0.8901	0.8610

made according to equation 2.22 when $x = 1$. Due to the minor improvement of the accuracy, the decision was made to not evaluate this processing further unless time would allow.

CFAR

For the CA-CFAR implementation the number of guard cells, N_G, was chosen to be two to cover the target's span in the data. The number of averaging cells, N_{CFAR}, was chosen to be five for reliable statistics of the noise surrounding the target.

The results when applying and training with CA-CFAR can be seen in table 4.14 for UC 2, 3 and the combination of the two. It can be seen that the CFAR algorithm increase the accuracy from 0.8932 to 0.8990 for UC 2 and for UC 3 the increase is from 0.8663 to 0.8732. Though not significantly increasing the performance of the blind spot detector it contributes to positive aspects. The parameter μ_{CFAR} is quite similar for the two UC whilst τ_{intra}

Table 4.14: The final settings and accuracy generated from the optimization of the CFAR algorithm using the Nelder-Mead algorithm. The optimization was made using UC 2 and 3, and lastly a combination of UC 2 and 3.

CFAR			
	UC 2	**UC 3**	**UC 2&3**
τ_{intra}	0.18	0.26	0.29
τ_{output}	0.16	0.11	0.12
μ_{CFAR}	0.53	0.58	0.48
Accuracy	0.8990	0.8732	0.8955

increased for both the UC 3 and for when the optimization was made using both UC. The increase of this factor leads to a higher degree of smoothing on the intra-frame output. From the recordings, it is clear that the signal is more slowly changing for UC 3 than for UC 2. At the same time, the τ_{output} is decreased.

Correlation of peaks

Using the correlation of peaks gave the results according to table 4.15. The peak interval of the previous frame which was cut out was set to be ± 2 indexes in depth to ensure that the entire target was enclosed. This was based on that the downsampling factor was set to 4, i.e. sampling every 24 cm in sparse service. Here one can see a similar set of parameter settings such that the one presented in 4.11, though now with the parameter τ_{output} approximately set to zero. The new parameter, μ_{corr}, becomes almost equally large for all three training sets. The accuracy is somewhat lower when using the correlation than without. However, when visually looking at the detection during the replay of the data it becomes clear that the correlation algorithm works as predicted and tracks the targets after the amplitudes are smaller than $v_{threshold}$. At the same time, other objects exceeding $v_{threshold}$ gets tracked longer and give rise to decreased performance.

In the video and data replay, when using the obtained parameters for the correlation, one can visually notice that the algorithm functions as predicted. It improved the detection and also the tracking of targets which had previously been detected by the threshold.

Table 4.15: The final settings and accuracy generated from the optimization of the correlation algorithm using the Nelder-Mead algorithm. The optimization was made using UC 2 and 3, and lastly a combination of UC 2 and 3.

Correlation			
	UC 2	**UC 3**	**UC 2&3**
τ_{intra}	0.16	0.16	0.17
$v_{threshold}$	1.62	1.62	1.68
μ_{corr}	0.20	0.19	0.20
Accuracy	0.8878	0.8654	0.8831

Combinations

Since both CFAR and correlation increased the performance, both were combined and the result is presented in table 4.16. All parameters change somewhat for each UC thought with a low spread. The accuracy increased further, though not much, compared to when only adding CFAR to the sparse processing algorithm. While training on UC 2 and 3 together the result is somewhat worsened from when using only CFAR. Looking at the playback of data, the combination performs visually better since the targets are more quickly detected and the correlation algorithm making the tracking better. At the same time, if noise occurs in the data, such as a lightning pole, it will be better tracked as well.

From the notion that the side sensors contains more noise such as bushes, buildings, lighting poles etc, the optimization was performed again with different parameter settings for the side and center sensors. The results can be

Table 4.16: The final settings and accuracy generated from the optimization of the combination of the CFAR and correlation algorithm using the Nelder-Mead algorithm. The optimization was made using UC 2 and 3, and lastly a combination of UC 2 and 3.

CFAR & Correlation			
	UC 2	**UC 3**	**UC 2&3**
τ_{intra}	0.29	0.24	0.27
μ_{CFAR}	0.57	0.65	0.60
μ_{corr}	0.31	0.12	0.13
Accuracy	0.9007	0.8739	0.8922

Table 4.17: The final settings and accuracy generated from the optimization of the combination of the CFAR and correlation algorithm using the Nelder-Mead algorithm. The optimization was made using UC 2 and 3, and lastly a combination of UC 2 and 3. The parameters were generated for the side sensors, S, and the center sensor, C.

CFAR, Correlation & Different settings						
	UC 2		**UC 3**		**UC 2&3**	
	C	**S**	**C**	**S**	**C**	**S**
τ_{intra}	0.26	0.23	0.25	0.24	0.27	0.24
μ_{CFAR}	0.55	0.64	0.55	0.65	0.56	0.66
μ_{corr}	0.12	0.12	0.11	0.12	0.11	0.12
Accuracy	0.8950		0.8751		0.8921	

seen in table 4.17. It can be seen that τ_{intra} and μ_{corr} becomes quite similar for both the center and side sensors for all UC. However, μ_{CFAR} differs since a higher threshold can be observed for the side sensors while a lower one is observed for the center. These settings resulted in the highest accuracy of UC 3 but the overall performance on the combination of the UC is not better. Therefore, the optimal algorithm which is used on the test data set is CFAR in combination with correlation. The parameters used continuously are the ones obtained in 4.16 where the optimization has been performed on the combination of the UC 2 and 3.

4.4.2 Validation of detection performance

Testing the optimally obtained sparse processing settings on UC 1 from table 4.11 on the test data, the accuracy of 0.9186 was obtained. This accuracy outperformed the performance on the training data which was 0.8944.

The obtained final processing for making the detections more robust was

Table 4.18: The resulting accuracy, sensitivity and specificity of the test data set with the proposed settings and post-processing.

	UC 1	**UC 2**	**UC 3**	**UC 2&3**
Accuracy	0.8903	0.8953	0.8938	0.8950
Sensitivity	0.5256	0.5486	0.8927	0.6112
Specificity	0.9677	0.9618	0.8943	0.9495

that of using CFAR and correlation of frames which settings can be seen in table 4.16. The result using these on the test data sets can be seen in table 4.18. The general sensitivity and specificity is added to the result on the different UC. The result shows a quite high specificity of all the UC with almost all close to 0.95. However, the sensitivity of UC 1, UC 2 and the combination UC 2 and 3 is quite low. Overall, the accuracy performance on the test data sets is equal to that of the training data sets.

Chapter 5
Discussion

The sensor characteristics which was evaluated resulted in a prototype consisting of three sensors angled 30° with respect to each other in the H-plane. The associated processing which comes with the sparse service was used with only the intra-frame part. To improve the robustness and accuracy of the processing both CFAR and correlation of peaks was used in the final solution. The motivations of all decisions will be further discussed in the following sections.

5.1 Sensor evaluation

5.1.1 Interference between sensors

From testing the interference of two sensors it was clear that the envelope service is heavily influenced by disturbances. These occurred as quick peaks, see figure 4.1, which were from direct leakage between the two sensors. While one of the sensors is transmitting the other receives this and registers as a large peak. This conclusion can be drawn from the fact that the shielding between the sensors removed this disturbance. Hence, shielding may be considered in the final product when using multiple sensors. For sparse, there is no clear disturbance which is why the test of shielding was not performed. Though there may be a disturbance in this service as well, it is seemingly not as heavily influenced. The disturbances are probably not as frequently occurring since the sparse service is much more seldom sampled with a lower duty cycle. If unforeseen disturbances occur for the sparse service in the future, shielding may be considered. Furthermore, using lenses did not affect the amount of disturbance occurring in either service which may be a result of this disturbance being direct leakage.[26]

The direct leakage of the sensor from the transmitter to the receiver is a well known problem. There are many proposed solutions to reduce this effect

such as using physical shielding, as used in this thesis, and Fourier processing as the disturbance is presented as a DC interference. Another solution could be to co-transmit the sensors simultaneously to reduce the chance of having a receiver picking up the direct radar content from the transmitters.

5.1.2 Angles of the radar beam

The radar beam characteristics show that it performs the best at close range to the sensors, while further away it is indicated that the radar beam becomes narrower. Both the H-plane and E-plane almost performs as stated in the specification at close ranges. This needs to be taken into consideration when generating further concepts to cover the wished area of the blind spot. Furthermore, the E-plane measurements slightly outperform the specifications when using a lens for both sparse and envelope service. The specification states the HPBW. The slightly underperforming angles could be because half the power is not enough to register any visual detection. From this result, the specifications are instead used as a guideline as of how the sensor approximately performs.

Sparse service tends to outperform the envelope service with a few degrees wider angular coverage. The reason for this may be due to that the sparse service sends multiple sweeps per frame with fewer depth points and therefore gets more chances to receive the targets reflections. Hence, it may only make the performance better at certain depths. More testing to find the explanation of this tendency is required but was not prioritized in this work.

5.1.3 Range of detection

Using a metal sheet as the target shows the importance of having a target with high permittivity, i.e. high RCS. This indicates that a human body is a bit worse in its ability to reflect the radar pulses as the metal slightly improved the angle for envelope. The level of visual detectability increased for the metal, but at the same time it was harder to focus and direct the beams back to the sensor since the metal at the same time could reflect the beams away from the sensor. This indicates that for a target with high permittivity, it does not directly mean a better signal strength due to the effect of spacial placing. Hence, it may occur that a car with a high permittivity surface could direct the beams away and thereby decrease the received reflections.

The calculation of the theoretical range assumed optimal circumstances and the result showed a possible distance of 5 meters. This is higher than what Acconeer had tested for while not using lenses for a pedestrian. However, the

range measurements showed a shorter range than the theoretical by 1 to 2 meters. The RCS is strongly dependent on the targets size, direction, clothing etc. which may explain the shorter ranges measured during the range evaluation. Though this calculated range indicates the possibility of using the sensor for the intended range. The measured range could become larger with the right settings and the right post-processing.

The used profile affected both the range of the sparse and envelope service. Since the aim was to achieve as large range as possible profile 4 was tested which showed an increase in the range. A larger number also decreases the depth resolution and since profile 4 functioned well, profile 5 was not evaluated since it would have reduced the depth resolution even further. The depth resolution cannot be too low since it may be of interest for the biker to have some sort of velocity estimation of the target approaching, this together with the capability of exact depth positioning. The system should still be ready for that sort of implementation if wanted in the future.

For the sparse service, the sampling mode B and a high sweeps-per-frame rate were desirable. The sampling mode B affects the sweep rate, being faster than mode A, and is theoretically better for detection of targets at larger ranges with smaller depth resolution than mode A. This aligns with the results. The high sweeps-per-frame rate can be motivated, as also mentioned in the results since the data then can capture more variations and generate a better estimation of the variance which is used to estimate the presence of the target.

For the envelope service, the downsampling factor increased the range and reduced the number of missed frames. When using the maximal downsampling factor 4, every fourth depth point is sampled instead of every frame when set to 1. Hence, the amount of data is reduced and the system is given more time to produce and process the frame, resulting in a reduction of the number of missed frames.

No apparent difference could be detected when using a biker and a pedestrian as targets. The difference in materials and placement of the person between the biker and a pedestrian could have affected the range. However, it seemed that the torso was the main reflector and that the small change of placement of the torso did not affect the reflectivity. The bike itself could have increased the range due to the change in the RCS. However, this was not the case and the reason may be that the metal of the bike facing the sensor often is rounded, making the radar beam reflection spread instead of being reflected towards the receiver. Since the main reflector seemed to be the torso of the biker, the eventual spread due to the bike did not noticeably affect the range of the detection.

The amount of missed frames proves that the needed range is too large for

the envelope service, even with maximal downsampling. The sensor cannot process the whole frame for all distances before the next frame needs to be processed. Hence, some frames are dismissed since the update rate was higher than the time of flight needed for the radar pulse to return to the sensor from the preset range. This results in many missed frames which means loss of information. The blind spot system needs to be able to function in real-time and, hence, there cannot be any missed frames. Since the sparse service is so sporadically sampled the system can keep up with the updating rate even though each frame consists of several sweeps. As sparse performs better in terms of missed frames it was chosen to be the service used for the final prototype.

5.2 Concept generation and evaluation

5.2.1 Blind spot definition

The blind spot definition generated for the biker is only based on the results from two persons, which is why it only can be used as a guideline rather than a final definition. For it to be reliable more tests have to be made for multiple ranges, with different bikes and mainly more test subjects to overcome the subjectivity. However, since the two test subjects are largely different in height, they at least can represent some variability. The worse performance compared to the expected coverage of peripheral vision could be because of the bikers positioning on the bike.

Allowing the biker a small tilt of the head or shift with the eyes is not said to influence the manoeuvring of the bike according to the two test subjects. Also, as the target would approach in the blind spot not covered by the sensors, it should previously have been detected by the sensors and notified the user before. Therefore, the main focus is to strive to cover the area behind rather than to the immediate sides.

5.2.2 Concept generation

The concept generation was restricted due to time limitations which is why not all potential placings and configurations of sensors were considered. The task was to generate a sensor package which could be placed on the bike. Placing the sensors too far back could potentially increase the sensor blind spot to the immediate sides but at the same time gain range. One solution could be to add a fourth sensor. The reason for placing the sensor package directly under the saddle rather than on the saddle post was due to the interference by the legs over the sensors. Again, more usability test has to be performed for

the final placement but the proposed positioning works without any greater disturbance.

The placement of the sensor influenced the raw data in one apparent matter; the bike itself is seen at approximately 0.4 meters. This is why the range was modified to start at 0.5 meters to not influence the detectability. Since targets that close to the bike would probably already have been noticed by the biker, either by sight or sound. Though, this test cannot prove whether the transmitted radar pulses after 0.5 meters is unaffected and reduced in signal power. However, no apparent effects of this can be seen and the range of detection during a quick test of this shows almost equal range. To determine if there is an effect, further testing is needed.

5.2.3 Concept evaluation

During the concept evaluation, some randomness could be seen in the data which was not predicted. One possible reason for this randomness may be due to inexact angling between the sensors when altering the prototype. The angles were determined with a protractor and some error between the actual value and expected value may have been present. Another possible reason may be the angling of the target to the radar beam. The visual detection seems to heavily depend on where the target was located in relation to the center of the beam. It becomes a balancing between good detection to the side but worse coverage far back, or early visibility far back with a bit worse coverage to the immediate side, see figure 4.5.

At the same time, the larger the angle was, the more perpendicular to the centers of the side sensors the target moved, and the harder the detection became. The pedestrian is thinner seen from the side than from the front or back resulting in a smaller RCS. Since the biker is more elongated from the side compared to the pedestrian, one would expect better detection but it is not. The bike may reflect the beams away from the receiver. Another reason is due to the shape of the beam since the sensor gap increases for larger angles. In other words, the largest reflection was made in the center of each sensor, and the larger the angle the larger the sensor gap became.

As previously mentioned in the results the range was shorter than predicted. The reason may be that the sparse service depends on movement, of either the target or the sensor. During these tests, the target may not have moved enough for the sensor to detect the target at the larger distances. This needs to be further evaluated to determine the cause of the decreased range.

H-plane evaluation

The final angling in the H-plane was chosen to be 30°. When the side sensors were angled 30° the sensors had no theoretical overlap and the gap between the sensor beams was small enough. Furthermore, the range of the sensors in this combination also almost fulfilled the needs of the blind spot angle covered, i.e. 100° backwards. A smaller angle between sensors would not have covered the whole area as wished. The sensor gap present at larger distances was also small enough to make it possible to track the target continuously due to the elongated shape of the targets. This was also the reason for not evaluating concepts with four sensors. Adding a fourth sensor is not needed since three sensors could cover the defined blind spot sufficiently. Using three sensors instead of four results in lower power consumption and less computational power which is desirable.

Lens holder

Furthermore, during the evaluation of the concepts no lens holder was used. Since small improvements of the consistency could be seen when using the lens holders. Hence, the previous results from the evaluation may be slightly unreliable due to the possible changes in the position of the lens over the sensor. The reason for using lens holder in the final concept was motivated by this improvement of the consistency and that the radar pattern better aligns with the theory. However, this may need more testing to be proven since the test for evaluating the lens holders only was made twice.

E-plane evaluation

Different angles in the E-plane was also evaluated. The purpose was to try to direct the beam towards the bikers torso since it previously was observed that the torso reflected the most. However, the angling of the sensors in the E-plane did not improve the results. It is possible that the angling rather directs the beam away from the biker instead of directing it towards the torso, worsening the results. Hence, the decision was made to not angle the sensors and to keep them in parallel with the ground.

Further evaluation of settings

The final test of the settings again confirmed the importance of profile 4 over 3. The range was somewhat lower for profile 3 than when using 4. The number of sweeps per frame was further increased to the maximal value of 42 before any missing frames occurred. It showed that increasing the number of sweeps

makes it easier to detect the target. There was no apparent difference between 32 and 42 sweeps per frame. This motivates why 32 was chosen since it reduced the amount of data and the risk of missing a frame compared to 42. Further tests may be required to confirm this and other values between 32 and 42 need to be evaluated. However, the best-found settings are used as the final sensor settings. These final obtained settings were optimized for the particular case of having a moving target, pedestrian or biker, and other settings may be needed for other products.

5.3 Data acquisition

5.3.1 The first user case

UC 1, which was the easiest, was not a realistic scenario but functioned as a scenario to prove the concept.

The annotation of ground truth of this UC was quite easy since it was clear where the target was situated due to the markings in the ground. The different movements recorded in this scenario was chosen to reflect common movements and cases covering positions which had been shown to be hard to detect. This would give a hint of the difficulty to detect the target at these positions.

5.3.2 The second user case

UC 2 is a more realistic scenario with the added disturbance of the bike itself moving. This may occur in a real-life situation, i.e. if the biker is travelling on a country road, on an empty cycle path etc. The moving pattern of the target in the blind spot intend to simulate real-life situations of how a target could cruise or approach in the blind spot. These patterns intended to be similar to the ones defined for UC 1 to be able to compare the results. The comparison was made to state if the movement of bike adds any difficulties for the detection.

Furthermore, some small errors may be present in the recording which was not intended, such as lampposts which can be seen in the video, though not a significant amount. It should not be there but as there is only a few the data was used as intended.

However, finding the exact positioning of the target was somewhat more difficult as the markings in the ground could not be achieved. The lace was used to provide some depth resolution in the video playback, but it could only provide an approximation of the depth for the side sensors. At the same time,

the rods were used to mark the transition between the sensors. This may have resulted in both length and sensor gap errors when annotating the ground truth. It was not as good conditions for generation of validation of this UC and a solution could be a video software for the estimation.

5.3.3 The third user case

UC 3 was the most realistic and true situation with regards to the intended use of the product. The aim of it was to capture different types of possible common disturbances. Moreover, it was still only a single main target present in the blind spot. The target was situated within the blind spot for the entire recording closing in and withdrawing, at different speeds and directions, to simulate real situations. Since the target was present within the 7 meters range during the whole recording this UC differs slightly from UC 1 and UC 2, where the target was present at further ranges. This could have influenced the results when using UC 3.

Furthermore, during this UC, the lace was not used to improve the depth resolution. The decision was made to exclude the lace since it could have been hazardous for the biker, the target or for others in the close surrounding. Hence, no reliable indication of the true range was available for UC 3. The only available guidelines were due to the use of the previously mentioned rods which indicated the angles of the direction of the sensor.

5.3.4 Annotation of ground truth

During the annotation of ground truth data, one problem was video and recording mismatch. The video started before the recording of raw data and needed to be trimmed for them to start simultaneously. The trimming may have lead to the video starting either slightly too early or too late. As a result, the training may have been done on wrongly annotated data. However, since the video was recorded in 360-degrees, capturing the entire scene, including the diodes, was making it possible to minimize the potential mismatch. The video could then be trimmed to start close to the indication of the diodes of started recording.

Another potential error source is that the ground truth may be biased due to the annotations being made manually. The manually made annotations could hold errors due to the visual determination of when the target should be detected, i.e. within 7 meters to the sensor. The visual determination of range and angles should be reliable for UC 1, but the annotation of UC 2 and 3 needs to be discussed. The depth resolution was a known problem, however, it

was hard to find a better solution due to limitation in resources and time. One solution to minimize this effect was made. The solution was to implement the possibility to pause and step forward 0.5 seconds in the recorded video and data. This made it possible to pause the video giving the person manually annotating more time to process the scene.

A future solution may be to use a better radar sensor as a golden standard. From that other radar, the exact positioning could be obtained making it possible to also validate the distance through mean square error. However, it may not be applicable for the use of bikes as it may be too costly or too large.

5.4 Detector optimization

The optimization algorithm chosen was the Nelder-Mead algorithm. It was found that the algorithm was sensitive to the initialization of the parameters to be trained. Some pre-testing of the different settings was needed to find an approximately good value for the parameters. Furthermore, the algorithms seemed to tend to get stuck in local maximums or plateau. This is a common problem during optimization and many other algorithms have been developed to handle this. Another limitation of the algorithm is that not all types of parameters could be trained. Some parameters could only hold integers and these could not be trained with the algorithm which tested values with several decimals. An other algorithm could be used for the optimization to avoid these problems.

It was found that the accuracy could be somewhat misleading. When evaluating the different results it became clear that the recorded sets of ground truth data was imbalanced and had a majority of true negatives, i.e. no target present. Hence, if the processing which was to be tested resulted in all negatives the accuracy could still be quite high. This would indicate an incorrect high accuracy which cannot be trusted. As an example, assume that the annotation contains 1/3 data of positives and 2/3 negatives. If the solution would state all negative, this would yield an accuracy of 66% which is relatively high. The processing aimed to increase the number of true positives and negatives, and not increase the number of false negatives. Hence, the results from the Nelder-Mead algorithm needed to be examined visually after optimization to determine if the processing had resulted in only negatives, providing a high but misleading result.

The problem of an imbalanced dataset is a well known within statistics and machine learning when optimizing the accuracy for a classifier. The emergence can be seen when evaluating the distribution of TP, TN, FP and FN.

There are several ways to overcome this problem and the most common is to alter the data set so that it becomes balanced. To obtain a balanced data set one can either oversample the minority or undersample the majority data set. Another possibility is to randomly sample equal amounts of data from each data set. One can also consider the idea to try to generate more data, either synthetically or through recording. As previously mentioned, there are many ways to approach this problem. Though, the distribution of recorded data in time seems quite balanced and the visual evaluation of post-processing playback show a solution that does not only find the solution which output only negatives. Further evaluation can be made to both find the distribution of positive and negative and to balance the data set during training. [27]

5.4.1 Optimization of detection algorithms

Sparse presence detection algorithm

The parameter w_{intra} was set to 1, resulting in no inter-frame procession of the data. This aligns with the theory, which states that the intra-frame part contains the information of fast movements within each frame. Hence, the detection is based on the variance within each frame and each depth to detect faster movements.

No intra-frame depth filter was used since no improvement of the accuracy could be seen and that the depth filtering may influence the estimation of the exact positioning of the target. Since the sensor data is very downsampled it reduces the impact of the depth filter, hence it may be motivated to use depth filtering if the downsampling would be smaller. The typical targets would then probably span over more than one depth point and the depth filter would then improve the estimation of the position. Therefore, depth filtering may still be considered for a future solution but needs to be tested for if it influences the positioning.

As mentioned in the results, the training set of UC 1 was decided to not be further used in the training. If UC 1 would be used during the training, it may have resulted in over-training which would give worse results for the other UC which include noise. UC 2 and UC 3 are more realistic recordings and should therefore be used to improved the robustness of the detection algorithm.

One possible reason for why the accuracy was not perfect even without noise could be that the video and data were not aligned during the annotation, this was however controlled and no major mismatch could be found for any of the recordings. Another possible reason may be that the processing is bad at detecting the target at larger ranges especially to the sides. UC 1 had a

high depth resolution in the video compared to the other UC. This may have resulted in more false negatives in the results of UC 1 since the detections start earlier in the ground truth. The annotation of the data for the other UC may be better due to a shorter detected range in the annotation, giving a better match between ground truth and the raw data. Furthermore, the reason could also be the lack of movement of the sensor itself during UC 1. The sparse service is found to potentially require some type of movement, of either the sensor or the target. Hence, the detection while using the sparse service may become better when both the sensor and the biker is moving to improve the range of the detection compared to UC 1.

Compensation of range

It was found that the only compensation which improved the results was the addition of the range times some factor. The reason may be since the intra-frame part holds information regarding the variance rather than the signal strength of the reflected radar pulse. It would therefore not follow the same proportionality as the radar equation describes.

Another solution could have been to detect several peaks and then sort them according to the largest reflection after compensation of only the chosen possible peaks and not the whole frame. This would probably not improve the detectability since the peaks still would need to be over the threshold to be detected, but it would rather improve the tracking of the strongest reflecting target. Acconeer has a similar solution for the distance detection applied to the envelope service.

CFAR

The implementation of CA-CFAR showed an increase in accuracy which indicates that the algorithm succeeds its purpose of an adaptive threshold. However, as the result is not much better one may consider using more advanced ways of estimating the threshold within a frame. One may also consider testing other number of guard cells, N_G, and averaging cells, N_{CFAR}, for the noise estimation level, as this heavily influences the threshold. The guard cells intend to cover the span of which the target is present in the data. It was assumed that the target spans five depth points, where two guard cells cover each side of the cell under test. The number of noise cells used is yet another parameter which can be used in further testing. Though, since the result improved, this algorithm and its settings were continued with.

The τ_{intra} and τ_{output} shows a tendency of when one being large, then the

other one is small and vice versa. This may be since the two averaging factors work in parallel, meaning that they together can result in an equal amount of averaging. Though, to confirm this further testing has to be performed. This difference in parameters may not result in huge accuracy drop when using the parameters obtained in one UC to that in another due to this relationship. However, it may indicate that two similar local minima of the optimization algorithm have been found.

Correlation of peaks

The correlation of peaks did not improve the accuracy compared to using only the sparse presence detect algorithm. However, it showed a tendency of working as intended. At the same time, this also applied to the false detection's, such as traffic lights etc present in UC 3, meaning that the false detections also was detected for a longer time resulting in an worsened accuracy. One solution to this problem could be to combine the correlation with some type of peak classification. The correlation could then be made only on peaks belonging to bikes, pedestrians and cars. It is common to use machine learning for classification in many different areas, such as image classification etc and it could be used to classify the peak [28]. However, this needs to be further investigated so pedestrians and bikers will not be removed resulting in more false negatives. Another solution could be to correlate the frame with a typical signal peak of a target of interest. This though requires recording more data of several bikes to get the best mean shape.

Another solution to reduce the number of false detections generated by the false targets could be to filter them out through their negative relative velocity. To determine if the target is non-moving the velocity of the biker could be used. If the measured relative velocity of the target is the same as the biker but negative, it could be said that the target has a zero velocity indicating that the target is static. This could then be used to filter out non-moving objects, reducing the number of false detection which are present in real biking scenarios which also would improve the accuracy for UC 3.

The fact that τ_{intra} is much higher than before could be because of the τ_{output} being set manually to almost zero. As discussed for CFAR, when one of them is low the other is high and this may be a result of this. Parameter τ_{output} was set to almost zero to obtain both quicker detections and faster drop of targets going under the threshold. Again, looking at the replay of data it seems to give much quicker detections and the drop seems fast but still gets tracked with the correlation, indicating that the correlation works. However, it needs more testing as the accuracy doesn't show this improvement since the

false positives also increase.

Correlation of peaks + CFAR

The combination of CFAR and the usage of correlation between peaks was slightly better than when using each type of processing individually. Again, the accuracy should, in theory, be slightly better than seen in the results. This is due to the same reason mentioned when using only correlation of peaks, i.e. the detection of false detection's are prolonged just as much as the true detections.

Correlation of peaks + CFAR + Sensor specific settings

While evaluating all results it was found that the center sensors have less noise and disturbances than the side sensors. Hence, the combination of CFAR and correlation was trained to find the optimal settings for both the side sensors and center sensor, i.e. sensor-specific settings. In the result of the training, it was easy to see that the center sensor converged to a lower threshold than the for the side sensors. This indicates that it is less noise and disturbances in the center sensor as predicted. The combination together with sensor-specific settings did not give the best general result, but it gave the best result for UC 3. Since it was not as general it was chosen to not be used. However, the thought of using sensor-specific processing is not entirely rejected due to the indication of less noise in the center sensor.

5.4.2 Validation of detection performance

The fact that the unseen test data either outperforms or performs equally to that of the trained data set indicates that no overtraining has occurred. The solution is therefore said to be generalized and can be used as a final prototype. For UC 1, the result of the test data is better which could be since the recorded training data may be affected by some unknown source of error. There may also be errors in the annotation of ground truth as previously discussed. Since UC 1 is not used in the further evaluation and as UC 2 and 3 performs equally this may not be a problem.

When further evaluating the final solution in regards of sensitivity and specificity on the test data set it generally showed that the specificity is higher than the sensitivity for all UC. The low sensitivity indicates that the optimization of accuracy has lead to that the detector has a hard time detecting all the positive cases but when it does it is sure of that. The high specificity indicates

instead that the false alarm rate is low, i.e. seldom outputs false positives. For UC 3 both sensitivity and specificity is quite high and may be because the solution is performing good. As discussed before, UC 3 is recorded with a target cruising around in the blind spot and due to the low depth resolution in video it may be faulty annotated, i.e. annotations starts at 6 meters instead of 7. Furthermore, the target is placed closer to the sensor during the major part of the recording than during the other UC's. Since the target is closer to the sensors, this could be one reason for the low sensitivity. The proposed solution may not be optimal for a seven meters range and may have to be reduced to e.g. five meters. Further tests to evaluate this needs to be performed. However, a reduction of the range is unwanted since the range needs to be as large as possible to have time to notify the biker. Another possibility is to test the detectors performance for certain ranges and validate against that instead of only the target being present or not within the set range. To summarize, the low sensitivity could be increased with the drawback of more false detections and one has to decide what is most important for the intended product.

5.5 Future development

The report has covered several types of concepts and types of processing, however, due to limitations in the thesis scope and the time restriction of the project the evaluation was also limited. Therefore, some proposals on further development and evaluation will be discussed. A discussion of the final prototype will then be followed and lastly, the conclusion of this thesis will be presented.

As discussed in previous sections, there is a need for further evaluation of the proposed types of processing. Different type of combinations needs to be done, where the range compensation could be used in combination with e.g. CFAR.

A more unspecific type of evaluation needed is to determine if the range can be further improved by the settings of the sensor and the processing, or if the sensor itself limits the range. This is a problem which should be prioritized to optimize the system even more. Some settings of the sensor can probably increase the range slightly, but no drastic improvements are expected. The sensor itself also seems limited to seven meters, further investigations in the code steering the sensors are needed to see if the range can be set to even further.

Another possible future implementation is some sort of relative velocity estimation. As mentioned when discussing correlation, the relative velocity

could be used to detect targets of interest. The relative velocity could also be of interest for the biker, where some notification could be done to indicate the speed of the approaching target. For example, show a red indication if the target detected is in the blind spot approaching fast, compared to yellow indicating the target going at constant relative speed etc.

Moreover, when the target is transitioning from one sensor to another at a far distance, the algorithm struggles to track the target. This is due to the design of the system which reset the tracking when the target leaves a filed of a sensor. The correlation cannot at the moment use a peak detected in one sensor to track peaks from another sensor. One solution is an addition to the algorithm making it possible to track the target through correlation after a transition to another sensor field. The range of the last detection made could be used to verify the transition to avoid false detections.

In this thesis, the focus was to try and implement as many computationally efficient algorithms as possible within the time frame of the project. The aim was to verify the effects of common types of algorithms used in radar rather than producing one or two types of processing and then improving them. For example, CFAR can be implemented in several ways, but only one type of implementation was tested in this report. With this method, it can be shown that using only small measures can improve the results. With further development within the types of processing suggested in this project it may result in even further increase in accuracy and a more robust system. However, more complex algorithms need to be evaluated so the system can keep up with the wished update rate. Higher complexity results in that higher computational power needed and that the processing gets more time-consuming. The system will need to be able to give the biker feedback in real-time, otherwise the purpose of the product cannot be fulfilled.

One aspect of the system which needs to be further discussed is whether it should be able to track one or several targets simultaneously. At the moment each sensor can only detect one target at the time. Since the proposed sensor setup has three sensors, the number of targets that can be detected simultaneously is three. The Acconeer sensor has theoretically a maximal range of 7 meters. Within the range of 7 meters, only 2-3 bikes will fit in a row. Side by side, 3-4 bikes will fit within the theoretical width of the sensor beam at seven meters and will then reduce as the distance to the sensors decreases. Hence, the available space is limited within the sensor coverage and the need of being able to detect several targets within these small ranges seems unimportant. The risk is that the system only will increase the number of false positive detection's.

Furthermore, since the sensor setup is composed of three sensors, the system can already detect at least three targets since the sensors at the moment

can detect one target at the time. The question is if it would be of importance for the biker to get notifications regarding more than three targets at the same time within the relatively small range? The biker may get overwhelmed with notifications if more targets than three would be detected simultaneously. One could argue that it is important to only notify the biker of the closest targets, since they are the closest and therefore the ones which are the most prominent to be hazardous.

Due to the system configuration the decision was made that the proposed processing would not need to be adapted to detect several targets. The focus was decided to rather be on how to make the detection more reliable instead of making it possible to detect several targets. However, this could need further testing to evaluate if it would improve the bikers experience of the system.

From the knowledge obtained in this thesis one may consider further testing of the current proposal of the blind spot detection system. The training of the processing should cover more of the cases which has been showed to be difficult for the system to handle. This could be seen as an extension to UC 3 scenario, i.e. biking in everyday traffic with multiple targets and disturbances. Also, it would be of interest of then adding some more difficult movements of the target, letting the target approach faster, more evaluation of the sensor gap at larger ranges, testing of the close range to the immediate sides etc. One should add the movement of the target moving in and out of the blind spot to better capture the detectability of new target, rather than tracking an already detected target. This movement was not as widely used in UC 3 in this thesis, but it should be covered from UC 2. This is also another reason for keeping UC 2 in the training. The new tests can be done according to the same method as before, i.e. with video recording to validate the ground truth, or through live feedback to the biker to capture the useability and the potential value it hopefully contributes. One may consider a combination of both as well in order to both train the system further and to evaluate the useability. It would be in this kind of test where the acceptable ratio of false detections over true positive detections is decided, i.e. is it of worth to detect all or be very sure of the result. In addition to accuracy one may also consider testing the sensitivity and specificity.

As for the physical prototype in terms of number of sensors, positioning, angling and so on, this may now be tested against the post-processing to see the detection output in real-time rather than making a visual detection of the raw data. It may be easier to classify the drawbacks and redefine which angling is to be used for the optimal setup. A more iterative process is to be considered where the prototype can be further developed based on the new post-processing and later on with this improved result the post-processing can

be done better for this new prototype. It was clear that using lens improves the range and makes the radar pattern more narrow. Design of new lenses for the intended use may be considered from this where it may not be as important to have a large E-plane. This can at the same time potentially reduce the effect of the bicycle rack as well, since the radar pulses then will be directed flat in the E-plane, i.e. less towards the ground and the sky. This may result in higher detectability to the sides which has been proven to be hard for an increased range.

The results from earlier testing when the target was a strong reflector, i.e. a metal sheet, showed difficulties in redirecting the radar pulses back to the receiver indicating that detecting cars would potentially be even harder. This under the assumption that the rounded shape of a car and its reflective surface is going to reflect the majority of the energy away. This though requires further testing and one might consider one of the other sensor modalities such as ultrasound. Again, one has to consider the need for detection of cars since the low range of the radar introduces the difficulty of being able to detect and warn the biker before the car has driven past due to the high velocity. The Garmin Varia radar can detect cars but has a much larger range. Hence, one could consider a combination of a radar with larger range places backwards together with the A111 sensor to the sides. Garmin Varia lacks the coverage of the blind spot close to the biker's sides since only one radar is used. Since the A111 has such low power consumption it could probably be combined with a sensor which has a larger consumption.

5.6 Ethics

Some aspects of this proposed product and its intended use gives reason to discuss the ethics. One needs to consider that the user could build up a false reliance in the product and therefore stops to utilize other senses to control the surroundings. Hence, a potential crash can occur if the blind spot detector were to miss a detection of a target approaching fast. This can occur from pure design and product flaws or from not knowing the limitations of the system. Another aspect is the ratio of false negatives and false positives where the user may consider the system being too sensitive or insensitive. This could happen if the system always gives notifications even if nothing is there or if it rejects true targets.

Furthermore, another thing to consider is the hackability of the product. With internet-of-things and connected devices comes the responsibility of preventing the product to be hackable which can result in product malfunctioning

or dangerous overtake of the system. Therefore it is of importance to take this into consideration during the development of the final system.

Radar technology also raises the question of how to handle interference between similar products transmitting in the same frequency band. Is it responsible to burden this unlicensed frequency band? We would say so since the purpose with the increased safety of the biker is both reduced community cost and personal damage. With the same argument of preventing bodily injury it is motivated to use this extension for every day biking even if it results in more environmental impact from production and increased power usage. However, this impact may in the end be small since the sensors are very power efficient.

5.7 Conclusions

In conclusion, the A111 sensor from Acconeer can be used in a blind spot detection system. It has been shown that these power efficient and small sensors can be used as a blind spot detector with a range of almost seven meters. The proposed setup consists of three sensors placed directly under the saddle. A 30° angle between the sensors is used to cover the defined blind spot of the biker and no angle in the E-plane is needed. The combination of CFAR and correlation of peaks is the chosen type of processing which makes the detection algorithm more robust. The sensor system works quite good, indicating its potential for the indented use with a quite high accuracy but with some limitations in range. However, more testing and development is needed to attain the final processing, sensor configuration and the final associated lenses to obtain a final product ready for deployment.

References

[1] Consumer Reports, "Car Safety & Efficiency" Feb. 2020 [online]. Available: https://www.consumerreports.org/issue/car-safety-efficiency?INTKEY=I000G0000.

[2] M. Hikita, "An introduction to ultrasonic sensors for vehicle parking." Feb. 2020 [online]. Available: http://www.newelectronics.co.uk/electronics-technology/an-introduction-to-ultrasonic-sensors-for-vehicle-parking/24966/.

[3] C. Fernández, D. Fernández-Llorca, M.-A. Sotelo, I. G. Daza, A. Hellín, and S. Alvarez, "Real-time vision-based blind spot warning system: Experiments with motorcycles in daytime/nighttime conditions," *International Journal of Automotive Technology*, vol. 14, 02 2013.

[4] Calamus, "Specifications." Feb. 2020 [online]. Available: https://calamusbikes.com/features.

[5] Nireeka, "Specifications." Feb. 2020 [online]. Available: https://nireeka.com/um/Nireeka-User-Manual-4May2019.pdf.

[6] M. Klotz, *An automotive short range high resolution pulse radar network.* Aachen, Germany: Shaker Verlag GmbH, 2002.

[7] Garmin, "Varia™ RTL511" May. 2020 [online]. Available: https://buy.garmin.com/sv-SE/SE/p/601468.

[8] M. Szinte and P. Cavanagh, "Apparent motion from outside the visual field, retinotopic cortices may register extra-retinal positions," *Plos One*,

10 2012. April. 2020 [online]. Available: https://journals.plos.org/plosone/article?id=10.1371/journal.pone.0047386.

[9] Avionics Department, *Electronic warfare and radar systems engineering handbook*. Point Mugu, California: Naval Air Warfare Center Weapons Division, 2013.

[10] Acconeer, "Radar sensor introduction." March. 2020 [online]. Available: https://acconeer-python-exploration.readthedocs.io/en/latest/sensor_introduction.html.

[11] Joint Range Instrumentation Accuracy Improvement Group, *Radar Loop Gain Measurements*. New Mexico, United States: Range Commanders Council, 1998.

[12] M. A. Richards, J. A. Scheer, and W. A. Holm, "Principles of modern radar: Basic principles." Feb. 2020 [online]. Available: https://m.eet.com/media/1111956/818_radar2.pdf.

[13] Acconeer, "Pulsed coherent radar" May. 2020 [online]. Available: https://www.acconeer.com/technology.

[14] Acconeer, "A111 - pulsed coherent radar (pcr), datasheet v2.1." March. 2020 [online]. Available: https://developer.acconeer.com/download/a111-datasheet-pdf/.

[15] Acconeer, "Getting started guide lens evaluation kit, may 2019." March. 2020 [online]. Available: https://developer.acconeer.com/download/getting-started-guide-lenses-pdf/.

[16] Acconeer, "Envelope." March. 2020 [online]. Available: https://acconeer-python-exploration.readthedocs.io/en/latest/services/envelope.html.

[17] M. S. Obaidat and P. Nicopolitidis, *Smart Cities and Homes: Key Enabling Technologies*. San Francisco, CA, United States: Morgan Kaufmann Publishers Inc, 2016.

[18] Acconeer, "Sparse." March. 2020 [online]. Available: https://acconeer-python-exploration.readthedocs.io/en/latest/services/sparse.html.

[19] Acconeer, "Presence detection (sparse)." April. 2020 [online]. Available: https://acconeer-python-exploration.readthedocs.io/en/latest/processing/presence_detection_sparse.html#presence-detection-sparse.

[20] P. P. Gandhi and S. A. Kassam, "Optimality of the cell averaging cfar detector," *IEEE Transactions on Information Theory*, pp. 1226–1228, July 1994.

[21] C. Wolff, "Constant false-alarm rate (cfar)." April. 2020 [online]. Available: https://www.radartutorial.eu/01.basics/False%20Alarm%20Rate.en.html#this.

[22] L. R. Rabiner and B. Gold, *Theory and Application of Digital Signal Processing*. PH, 1975.

[23] H. L. Sneha, "Understanding correlation." May. 2020 [online]. Available: https://www.allaboutcircuits.com/technical-articles/understanding-correlation/.

[24] M. Yasugi, Y. Cao, K. Kobayashi, T. Morita, T. Kishigami, and Y. Nakagawa, "79ghz-band radar cross section measurement for pedestrian detection," *2013 Asia-Pacific Microwave Conference Proceedings (APMC), Seoul*, pp. 576–578, 2013.

[25] The Auto Prophet, "Side View Mirror Setting." May. 2020 [online]. Available: http://theautoprophet.blogspot.com/2007/07/side-view-mirror-setting.html.

[26] J. Byrnes, "Advances in sensing with security applications." May. 2020 [online]. Available: https://www.researchgate.net/publication/270579557_Advances_in_Sensing_with_Security_Applications_Wireless_sensor_networks_for_security_issues_and_challenges.

[27] A. Mahani and A. R. B. Ali, "Classification problem in imbalanced datasets, recent trends in computational intelligence." June 2020 [online]. Available: https://www.intechopen.com/books/recent-trends-in-computational-intelligence/classification-problem-in-imbalanced-datasets.

[28] S. Russel and P. Norvig, *Artificial intelligence - a modern approach (Third edition)*. Edinburgh Gate, Harlow, Essex Cm20 2JE, England: Pearson Education Limited, 2016. Global edition. ISBN 13: 978-1292153964.

Appendix

Table 5.1: The settings used when measuring and evaluating the angles of the radar beam using the envelope service.

Settings for envelope service	
Range interval (m)	0.3 - 2.0
Profile	3
Update rate (Hz)	30
Running average factor	0.7
Repetition mode	Host driven
Downsampling factor	1
HW acceleration average samples	15
Gain	0.5
Noise level normalization	Enabled

Table 5.2: The settings used when measuring and evaluating the angles of the radar beam using the sparse service.

Settings for sparse service	
Range interval (m)	0.3 - 2.0
Profile	3
Update rate (Hz)	60
Sweep rate (Hz)	3000
Sweeps per frame (Hz)	16
Sampling mode	B
Repetition mode	Host driven
Downsampling factor	1
HW acceleration average samples	63
Gain	0.5

Table 5.3: The default settings used when measuring the range using the envelope service.

Default settings for envelope service	
Range interval (m)	0.5 - 7.0
Profile	3
Update rate (Hz)	30
Running average factor	0.7
Repetition mode	Host driven
Downsampling factor	1
HW acceleration average samples	15
Gain	0.5
Noise level normalization	Enabled

Table 5.4: The default settings used when measuring the range using the sparse service.

Default settings for sparse	
Range interval (m)	0.5 - 7.0
Profile	3
Update rate (Hz)	60
Sweep rate (Hz)	3000
Sweeps per frame (Hz)	16
Sampling mode	B
Repetition mode	Sensor driven
Downsampling factor	4
HW acceleration average samples	63
Gain	0.5

Table 5.5: The ”optimal” settings used when measuring the range using the envelope service.

Settings for ”optimal ”envelope	
Range interval (m)	0.5 - 3.5 without lens 0.5 - 7 with lens
Profile	4
Update rate (Hz)	30
Running average factor	0.7
Repetition mode	Host driven
Downsampling factor	4
HW acceleration average samples	32
Gain	0.5
Noise level normalization	Enabled

Table 5.6: The ”optimal” settings used when measuring the range using the sparse service. The same settings were used for the recording of the user cases.

Settings for ”optimal” sparse	
Range interval (m)	0.5 - 7.0
Profile	4
Update rate (Hz)	60
Sweeps per frame (Hz)	32
Sampling mode	B
Repetition mode	Sensor driven
Downsampling factor	4
HW acceleration average samples	63
Gain	0.5

Table 5.7: The angles at different radii where the target is leaving the field of detection for the center and one of the side sensors. Target was a pedestrian and the measurements was made for different angles between the sensors.

		45°	**40°**	**35°**	**30°**	**25°**
Center edge	**3 m**	40°	35°	30°	25	30
	5 m	25°	20°	20°	15°	25°
	6.5 m	10°	10°	15°	10°	10°
Side inner edge	**3 m**	50°	30°	30°	20°	30°
	5 m	70°	50°	45°	45°	35°
	6.5 m	50°	55°	45°	30°	-
Side outer edge	**3 m**	80°	70°	70°	50°	65°
	5 m	80°	65°	55°	65°	60°
	6.5 m	55°	55°	45°	35°	-

Table 5.8: The angles at different radii where the target is leaving the field of detection for the center and one of the side sensors when lens holders are used. Target was a pedestrian and the measurements was made twice.

		1	2
Center edge	**3 m**	15°	25°
	5 m	10°	10°
	6.5 m	5°	10°
Side inner edge	**3 m**	15°	20°
	5 m	20°	20°
	6.5 m	20°	25°
Side outer edge	**3 m**	40°	40°
	5 m	35°	35°
	6.5 m	35°	30°

Table 5.9: The range intervals where the target was barely visible (BV) and visible (V) for the side (S) and center (C) sensors, for 30°between the sensors in the H-plane when lens holders are used. The measurements were made twice when the target was a pedestrian (P) and a biker (B).

		P 1		**P 2**		**B 1**		**B 2**	
		BV	**V**	**BV**	**V**	**BV**	**V**	**BV**	**V**
C	**0.5 m**	6-0.5	4-1	6-1	3-1	5-1	3-1	4.5-2	3.5-3
	1.0 m	-	-	-	-	-	-	-	-
	1.5 m	-	-	-	-	-	-	-	-
	2.0 m	-	-	-	-	-	-	-	-
	2.5 m	-	-	-	-	-	-	-	-
S	**0.5 m**	2-0.5	2-0.5	2-0.5	2-0.5	1.5-0.5	1.5-0.5	2.5-0.5	2.5-0.5
	1.0 m	2.5-1	2.5-1	3.5-1	2.5-1	2.5-1.5	2.5-1.5	2.5-1	2.5-1
	1.5 m	4-2.5	3-2.5	4.5-2	4-2	3.5-2	3-2.5	3.5-2.5	3.5-2.5
	2.0 m	5-3	3.5-3	4.5-3	4-3	4.5-4	-	-	-
	2.5 m	5-4	-	5-4	-	.	-	-	-

Table 5.10: The range intervals where the target was barely visible (BV) and visible (V) for the side (S) and center (C) sensors for different angles between the sensors in the H-plane. The target was a pedestrian and the measurements was made for different angles between the sensors.

		45°		**40°**		**35°**		**30°**		**25°**	
		BV	**V**	**BV**	**V**	**BV**	**V**	**BV**	**V**	**BV**	**V**
C	**0.5 m**	5 -	3-0.5	3-0.5	2-0.5	4.5-0.5	4-0.5	4-1	2-1	4-0.5	3-0.5
	1.0 m	2.5-1	-	-	-	4.5-1.5	2.5-2	-	-	2-1.5	2-2
	1.5 m	-	-	-	-	-	-	-	-	-	-
	2.0 m	-	-	-	-	-	-	-	-	-	-
	2.5 m	-	-	-	-	-	-	-	-	-	-
S	**0.5 m**	1.5 -	1.5-0.5	2-0.5	2-0.5	2-0.5	1.5-0.5	2.5-0.5	2-0.5	2-0.5	2-0.5
	1.0 m	2-0.5	2-1	1.5-1	1.5-1	2-1	2-1	3-1	2.5-1.5	2.5-1	2-1.5
	1.5 m	3-2	2.5-2	3-2	2.5-2	3-1.5	2.5-2	3.5-2.5	-	3-2	3-2
	2.0 m	4-3	3.3-3	3.5-2.5	3-2.5	3.5-2.5	3-2.5	3.5-3	-	4-3	-
	2.5 m	4-3	3.5-3	4-3	3.5-3.5	4-3	-	-	-	5-3.5	-

Table 5.11: The range intervals where the target was barely visible (BV) and visible (V) for the side (S) and center (C) sensors for different angles between the sensors in the H-plane. The target was a biker and the measurements was made for different angles between the sensors.

		45		**40**		**35**		**30**		**25**	
		BV	**V**	**BV**	**V**	**BV**	**V**	**BV**	**V**	**BV**	**V**
C	**0.5 m**	3.5-0.5	3-0.5	3-0.5	1-1	5.5-1	4-1	3-0.5	3-0.5	4-0.5	3-0.5
	1.0 m	3-2	-	-	-	5-4.5	-	-	-	-	2-2-
	1.5 m	-	-	-	-	-	-	-	-	-	-
	2.0 m	-	-	-	-	-	-	-	-	-	-
	2.5 m	-	-	-	-	-	-	-	-	-	-
S	**0.5 m**	1.5-0.5	1.5-0.5	1.5-0.5	1.5-0.5	2-0.5	2-0.5	2-0.5	2-0.5	2-0.5	1.5-0.5
	1.0 m	2.5-1	2-1	2-1	2-1	2.5-1	1.5-1	3-1.5	2.5-1.5	3-1	2.5-1
	1.5 m	3.5-2	3-2	2.5-1.5	2-2	3-1.5	2-1.5	3-2	3-2	3.5-1.5	3-1.5
	2.0 m	4-2.5	3.5-3	3.5-2.5	3-3	3.5-3	-	4.5-3	-	3.5-3	-
	2.5 m	4.5-3.5	4-4	4-3.5	-	4.5-3.5	4-3.5	-	-	-	-

Table 5.12: The range intervals where the target was barely visible (BV) and visible (V) for the side (S) and center (C) sensors. The measurements were made with both a pedestrian (P) and a biker (B) as a target. The angles evaluated were both 5 and 10 degrees in the E-plane. The angle was 30 degrees in the H-plane.

		5°				**10°**			
		P		**B**		**P**		**B**	
		BV	**V**	**BV**	**V**	**BV**	**V**	**BV**	**V**
C	**0 m**	6.5-0.5	5.5-0.5	6.5-0.5	5.5-0.5	6-0.5	5-0.5	5.5-0,5	5-0.5
	0.5 m	2-1.5	-	5.5-1	-	5.5-1	2-1	-	-
	1.0 m	-	-	-	-	-	-	-	-
	1.5 m	-	-	-	-	-	-	-	-
S	**0 m**	-	-	-	-	1-1	1-1	-	-
	0.5 m	2.5-0.5	2-0.5	2.5-0.5	2.5-0.5	2-0.5	2.0.5	2-0.5	2-0.5
	1.0 m	3.5-1.5	3-1.5	3.5-1.5	3-1.5	3.5-1.5	3-1.5	3.5-1.5	3-1.5
	1.5 m	4.5-2.5	4-2.5	4.5-2.5	4-2.5	4.5-2.5	3.5-2.5	4.5-2.5	4-2.5

Table 5.13: The range intervals where the target was barely visible (BV) and visible (V) for the side (S) and center (C) sensors during different settings (1-3).

		1		**2**		**3**	
		BV	**V**	**BV**	**V**	**BV**	**V**
C	**0.5 m**	-	-	-	-	-	-
	1 m	-	-	-	-	-	-
	1.5 m	-	-	-	-	-	-
S	**0.5 m**	2.5-0.5	2-0.5	2.5-0.5	2-0.5	2.5-0.5	2-0.5
	1 m	4-1.5	3-1.5	4-1.5	3.5-1.5	3.5-1.5	3-1.5
	1.5 m	4-2.5	4-2.5	5-2	4.5-2	4-2.5	3.5-2.5